UAV-Aided Two-Way Multi-User Relaying

Zhichao Sheng, Hoang Duong Tuan, Trung Q. Duong, and Lajos Hanzo

Abstract—Unmanned aerial vehicle (UAV)-aided two-way relaying networks are designed, where a UAV is deployed to assist multiple pairs of users in their information exchange. There are two basic approaches for the user pairs' information exchange within a single time slot via the UAV relay. The first approach is based on full-duplex, where all participants operate in the full-duplex mode to transmit and receive signals simultaneously. However, all transceivers have to operate in the face of severe self-interference, which cannot be completely suppressed. The second approach is based on conventional half-duplex, where the users send their information to the UAV within a certain fraction of the time slot, and the UAV relays them within the remaining fraction to avoid the self-interference. In either approach, the joint bandwidth and power allocation maximizing the sum information exchange throughput under realistic resource and user throughput constraints poses a complex nonconvex problem. New inner approximations are proposed for developing path-following algorithms for their computation. Our numerical results show that the time-fraction-based half-duplex approach clearly outperforms the high-complexity full-duplex approach.

Index Terms—Unmanned aerial vehicle (UAV)-enabled communication, two-way relaying, throughput optimization, nonconvex optimization.

I. INTRODUCTION

Unmanned aerial vehicles (UAVs) are capable of supporting and/or replacing the communication infrastructure in case of disasters, battlefields or sporting events, thanks to their high mobility, configuration flexibility and cost-efficiency [1]–[5]. Hence the research of UAV-enabled communication has attracted a lot of recent attention (see e.g. [1]–[9] and references therein). A UAV was exploited as a flying base station (BS) for

Z. Sheng was with the school of the School of Electronics, Electrical Engineering and Computer Science, Queen's University Belfast, Belfast BT7 1NN, U.K. He is now with Key Laboratory of Specialty Fiber Optics and Optical Access Networks, Joint International Research Laboratory of Specialty Fiber Optics and Advanced Communication, Shanghai University, Shanghai 200444, China (email: zcsheng@shu.edu.cn).

H. D. Tuan is with the school of Electrical and Data Engineering, University of Technology, Sydney, NSW 2007, Australia (email: tuan.hoang@uts.edu.au).

T. Q. Duong is with the school of the School of Electronics, Electrical Engineering and Computer Science, Queen's University Belfast, Belfast BT7 1NN, U.K. (email: trung.q.duong@qub.ac.uk).

L. Hanzo is with the school of Electronics and Computer Science, University of Southampton, Southampton, SO17 1BJ, U.K. (e-mail: lh@ecs.soton.ac.uk)

serving multiple downlink (DL) users, where the joint design of the UAV's altitude and beamwidth or the joint design of transmit power, bandwidth, transmit rate, and UAV's position was proposed in [10] and [11], respectively for maximizing the sum throughput. Similarly, the joint design of bandwidth allocation, power allocation, the UAV's altitude and transmit antenna beamwidth was considered in [12] for maximizing the users' worst throughput under non-orthogonal multiple access (NOMA). In [13], the authors considered the two-way communication of multiple UAV-user links, which was implemented by appropriately adapting the transmission directions of each link. In [14], a full-duplex (FD) secrecy communication scheme was proposed, where the energy efficiency of secrecy communication was maximized by joint the design of UAV trajectory and UAV/source transmit powers. Exploiting a UAV as a flying relay for two-hop communication between a source and destination, the joint design of the UAV trajectory and the transmit power was proposed in [15] for maximizing the throughput. By contrast, the authors of [16] aimed for minimizing the outage probability, while the authors of [17] have improved both the fairness and the energy efficiency. The placement of multiple UAVs for either multi-hop single links or for multiple two-hop links between a source and destination was considered in [18] by maximizing the end-to-end signal-to-noise ratio. The associated radio resource optimization was considered in [19] for supporting the time division long-term evolution advanced (TD-LTE-A) standard with the aid of multiple UAV-assisted relaying.

Two-way relaying (TWR) is capable of supporting information exchange between users in two steps [20]–[24]. Various UAV-aided TWR systems were considered in [25], [26]. Explicitly in [25], the joint design of UAV position and transmission power optimization was used for maximizing the sum rate, while in [26] the minimum average rate maximization was considered by the joint design of the UAV trajectory, transmit power and bandwidth. However, the information exchange in [25], [26] is arranged via half-duplex (HD) operation. Furthermore, the deployment of FD [27]–[33] at all nodes using separate transmit and receive antennas for simultaneous signal transmission and reception dispenses with separate transmit/receive time slots. However, the main impediment of this FD-based approach is the hostile self-interference (SI) imposed by the co-location of the transmit and receive antennas. Although there is encouraging research progress in suppressing the SI, it is still an open challenge to ensure that FD-based TWR outperforms the classic HD-based TWR in terms of spectral efficiency [34], [35]. The solution advocated in [36], [37] is the first one making TWR within a single time slot implementable based on the conventional HD solution. Explicitly, the users transmit their information to the relays within a certain fraction of the time slot (TS),

TABLE I: A brief comparison of the related literature.

Contents \ Literature	This work	[10]–[14]	[15]–[19]	[25]	[26]
BS		✓			
One-way relaying			✓		
HD-based TWR	✓			✓	✓
One two-way pair					✓
Multiple two-way pairs	✓			✓	
FD-based TWR	✓				
BP-based TWR	✓				
TF-based TWR	✓				
Bandwidth allocation	✓				

and then the relays forward the signal to the users during the remaining fraction of the TS, hence only requiring a single antenna for both transmission and reception, whilst dispensing with SI. The benefit of fractional time allocations in terms of improving the capacity of single-user and single-input single output HD decode-and-forward systems has been shown earlier e.g. in [38], [39]. To sum up, we provide a brief comparison of the related literature in Table I.

Against this background, this paper investigates a UAV-aided TWR communication network, where a UAV relay helps multiple pairs of users to exchange their information within one time slot. In order to avoid inter-pair interference, each pair of users is allocated a sliver of communication bandwidth. Additionally, the location of the UAV can be optimized offline and then be fixed to save propulsion energy [40]. We aim for jointly optimizing both the bandwidth and power allocation for maximizing the sum of information exchange throughput subject to the constraints of the power budget, total bandwidth, as well as the users' minimum required throughput. The contributions of this paper are as follows.

- To address this constrained optimization problem with the aid of a FD-based interface, which is nonconvex and hence computationally challenging, we develop new inner approximation techniques, which lead to an efficient path-following procedure for its solution.
- For time-fraction (TF)-based and HD-based transmission, this constrained optimization problem involves the additional decision variable of TF, which changes the nature of the throughput functions involved. Hence, we propose new inner approximation techniques to develop a bespoke path-following algorithm for solving the problem. The numerical results show that the TF-based approach outperforms both the FD-based and the conventional HD-based TWR techniques.

The rest of this paper is organized as follows. Section II is devoted to FD-based TWR, under which each user pair is allocated a communication bandwidth for their TWR. Then Section III considers a pair of HD-based TWR schemes, which are still implementable within a single time-slot. In the first one, similarly to the FD TWR each user pair is also allocated a communication bandwidth but they send their signals to the UAV relay in the first half of the time slot and receive their signal from the UAV relay in the second half of the time slot. By contrast, in the second particular case each user transmits and receives his/her signal over separate bandwidths, so there is still no FD SI. Section IV is devoted to TF-aided HD-based

TWR, where each user pair is allocated a communication bandwidth and they send as well as receive their signal over the same allocated bandwidth within the allocated time-fractions of the time-slot. In contrast to the first particular case of Section III, where the time-fractions were fixed to $1/2$, they are now also optimized. The simulations carried out in Section V show the clear advantage of the TF-aided TWR over its counterparts. Our conclusions are drawn in Section VI. The appendices provide the fundamental inequalities used in the derivation of the algorithms.

Notation. $n \sim \mathcal{CN}(\bar{n}, \sigma)$ indicates that n is a circularly-symmetric complex Gaussian random variable with a mean of $\bar{n}$ and variance of σ. The optimization variables are printed in boldface.

II. FULL-DUPLEX BASED UAV-ENABLED TWR

Consider a UAV-aided TWR communication network with two groups of ground users as depicted by Fig. 1. Each ground user (UE) $k \in \{1, \ldots, K\}$ is paired with UE $\pi(k) = K+k$ for information exchange. We assume that there is no direct link between the two UE groups, so UE k and UE $\pi(k) = K + k$ exchange information with each other via the UAV relay.
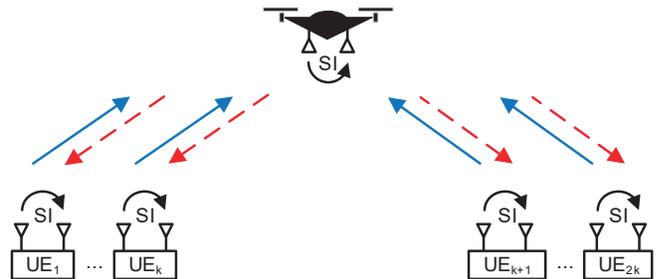
Fig. 1: FD-based TWR

Let $\mathcal{B}$ be the normalized bandwidth, which can be shared among the UEs, so that two way communication between UE k and UE $\pi(k)$ is supported by using a fraction

$$b_k = 1/\tau_k, \quad k = 1, \ldots, K, \tag{1}$$

of $\mathcal{B}$, where $0 \leq 1/\tau_k \leq 1$ is the fraction of the bandwidth. Let h_k and g_k be the ground-to-air (G2A) channel and air-to-ground (A2G) channel between UE k and the UAV, respectively,

In FD TWR communication, the UAV and UEs operate in the FD mode. In support of this, each node has two antennas,

one of the antennas is for signal transmission, while the other is for signal reception.

Let s_k and $s_{\pi(k)}$ represent the information symbol transmitted by UE k and UE $\pi(k)$, respectively, which are independent and normalized, i.e., $\mathbb{E}(|s|_k^2) = \mathbb{E}(|s|_{\pi(k)}^2) = 1$. Let us furthermore define p_k^2 and $p_{\pi(k)}^2$ as the power allocated to s_k and $s_{\pi(k)}$, respectively. Accordingly, the signal received by the UAV over the bandwidth $1/\tau_k$ can be written as

$$r_k = h_k p_k s_k + h_{\pi(k)} p_{\pi(k)} s_{\pi(k)} + e_{LI,k} + n_{R,k}, \quad (2)$$

where $e_{LI,k}$ models the effect of analog circuit imperfections and the limited dynamic range of the analog-to-digital converter (ADC) at the UAV, $n_{R,k} \sim \mathcal{CN}(0, \sigma_{UAV}/\tau_k)$ is the background noise at the UAV with $\sigma_{UAV} = \sigma_n^2$, and σ_n^2 is the noise power density.

The maximum allowed transmit power of UEs is constrained by $P^{U,\max}$, i.e.

$$p_k \leq \sqrt{P^{U,\max}}, \ 1 \leq k \leq 2K. \quad (3)$$

In order to restrict the interference imposed on neighboring networks, the total transmit power of UEs is limited by

$$\sum_{k=1}^{2K} p_k^2 \leq P_{\text{sum}}^{U,\max}. \quad (4)$$

The UAV processes the received signal and retransmits it by allocating the power fraction $1/p_{R,k}$ to it

$$\frac{r_k}{\sqrt{p_{R,k}}} = \frac{1}{\sqrt{p_{R,k}}} \left(h_k p_k s_k + h_{\pi(k)} p_{\pi(k)} s_{\pi(k)} + e_{LI,k} + n_{R,k} \right).$$

Let $\boldsymbol{\tau} \triangleq \{\tau_k, k = 1, \ldots, \tau_K\}$ and $\mathbf{p} \triangleq \{(p_k, p_{\pi(k)}, p_{R,k}), k = 1, \ldots, K\}$. Then the transmit power at the UAV over the bandwidth $b_k = 1/\tau_k$ can be expressed as

$$P_k^A(\boldsymbol{\tau}, \mathbf{p}) = \frac{1}{p_{R,k}(1 - \sigma_{SI}^2)} \left(|h_k|^2 p_k^2 + |h_{\pi(k)}|^2 p_{\pi(k)}^2 + \frac{\sigma_{UAV}}{\tau_k} \right), \quad (5)$$

which is constrained by $P^{A,\max}$ as

$$P_k^A(\boldsymbol{\tau}, \mathbf{p}) \leq P^{A,\max}, \ 1 \leq k \leq K. \quad (6)$$

For simplicity, in line with [36] we assume that $e_{LI,k}/\sqrt{p_{R,k}} \sim \mathcal{CN}(0, \sigma_{SI}^2 P_k^A(\boldsymbol{\tau}, \mathbf{p}))$, where σ_{SI} is the UAV channel's instantaneous residual SI attenuation level, hence we have

$$\mathbb{E}(|e_{LI,k}|^2) = \frac{\sigma_{SI}^2}{1 - \sigma_{SI}^2} \left(|h_k|^2 p_k^2 + |h_{\pi(k)}|^2 p_{\pi(k)}^2 + \frac{\sigma_{UAV}}{\tau_k} \right). \quad (7)$$

Moreover, the sum transmit power of the UAV is also limited by $P_{\text{sum}}^{R,\max}$:

$$
\begin{aligned}
P_{\text{sum}}^R(\boldsymbol{\tau}, \mathbf{p}) &= \sum_{k=1}^K P_k^A(\boldsymbol{\tau}, \mathbf{p}) \\
&= \sum_{k=1}^K \frac{1}{p_{R,k}(1 - \sigma_{SI}^2)} \left(|h_k|^2 p_k^2 + |h_{\pi(k)}|^2 p_{\pi(k)}^2 \right. \\
&\qquad\qquad \left. + \frac{\sigma_{UAV}}{\tau_k} \right) \\
&\leq P_{\text{sum}}^{R,\max}.
\end{aligned}
\quad (8)
$$

The UAV forwards the processed signals to all UEs and then the signals received at UE k and $\pi(k)$ are given by

$$
\begin{aligned}
y_k =\ &\frac{g_k}{\sqrt{p_{R,k}}} \left(h_k p_k s_k + h_{\pi(k)} p_{\pi(k)} s_{\pi(k)} + e_{LI,k} + n_{R,k} \right) \\
&+ \chi_{k,k} p_k \tilde{s}_k + n_k,
\end{aligned}
\quad (9)
$$

and

$$
\begin{aligned}
y_{\pi(k)} =\ &\frac{g_{\pi(k)}}{\sqrt{p_{R,k}}} \left(h_k p_k s_k + h_{\pi(k)} p_{\pi(k)} s_{\pi(k)} + e_{LI,k} + n_{R,k} \right) \\
&+ \chi_{\pi(k),\pi(k)} p_{\pi(k)} \tilde{s}_{\pi(k)} + n_{\pi(k)},
\end{aligned}
\quad (10)
$$

where $\chi_{k,k} \tilde{s}_k$ and $\chi_{\pi(k),\pi(k)} \tilde{s}_{\pi(k)}$ respectively denote the FD interference at UEs k and $\pi(k)$ with $|\chi_{k,k}|^2 = |\chi_{\pi(k),\pi(k)}|^2 = \sigma_{SI}^2$, and $n_k \sim \mathcal{CN}(0, \sigma_{UE}/\tau_k)$ and $n_{\pi(k)} \sim \mathcal{CN}(0, \sigma_{UE}/\tau_k)$ are the background noise at the receiver of UEs k and $\pi(k)$ with $\sigma_{UE} = \sigma_n^2$.

We can rewrite (9) and (10) as

$$
\begin{aligned}
y_k =\ &\frac{g_k}{\sqrt{p_{R,k}}} h_{\pi(k)} p_{\pi(k)} s_{\pi(k)} + \frac{g_k}{\sqrt{p_{R,k}}} h_k p_k s_k \\
&+ \frac{g_k}{\sqrt{p_{R,k}}} \left(e_{LI,k} + n_{R,k} \right) + \chi_{k,k} p_k \tilde{s}_k + n_k,
\end{aligned}
\quad (11)
$$

and

$$
\begin{aligned}
y_{\pi(k)} =\ &\frac{g_{\pi(k)}}{\sqrt{p_{R,k}}} h_k p_k s_k + \frac{g_{\pi(k)}}{\sqrt{p_{R,k}}} h_{\pi(k)} p_{\pi(k)} s_{\pi(k)} \\
&+ \frac{g_{\pi(k)}}{\sqrt{p_{R,k}}} \left(e_{LI,k} + n_{R,k} \right) + \chi_{\pi(k),\pi(k)} p_{\pi(k)} \tilde{s}_{\pi(k)} \\
&+ n_{\pi(k)},
\end{aligned}
\quad (12)
$$

where the first terms of their right-hand sides (RHSs) are the desired signal components. The second terms represent self-interference, which can be mitigated by estimating leakage channel of both the forward and backward channels as well as the allocated power and then reconstructing as well as substituting the estimated SI. The last two terms represent the background noise. It is worth noting that there is no inter-pair interference in the received signals, since the communication between the users of each pair of is carried out over their dedicated bandwidth.

When invoking (11), (12), and (7), the signal-to-interference-plus-noise ratio (SINR) at UE k and $\pi(k)$ after respectively removing the self-interference term $g_k h_k p_k s_k/\sqrt{p_{R,k}}$ and $g_{\pi(k)} h_{\pi(k)} p_{\pi(k)} s_{\pi(k)}/\sqrt{p_{R,k}}$ is then

calculated as

$$\gamma_k(\boldsymbol{\tau}, \mathbf{p}) = |h_{\pi(k)}|^2 p_{\pi(k)}^2 \bigg/ \bigg[\frac{\sigma_{SI}^2}{1 - \sigma_{SI}^2}$$

$$\times \left(|h_k|^2 p_k^2 + |h_{\pi(k)}|^2 p_{\pi(k)}^2 + \frac{\sigma_{UAV}}{\tau_k} \right)$$

$$+ \frac{\sigma_{UAV}}{\tau_k} + \frac{\sigma_{SI}^2}{|g_k|^2} p_{R,k} p_k^2 + \frac{\sigma_{UE}}{|g_k|^2} \frac{p_{R,k}}{\tau_k} \bigg], \quad (13)$$

and

$$\gamma_{\pi(k)}(\boldsymbol{\tau}, \mathbf{p}) = |h_k|^2 p_k^2 \bigg/ \bigg[\frac{\sigma_{SI}^2}{1 - \sigma_{SI}^2}$$

$$\times \left(|h_k|^2 p_k^2 + |h_{\pi(k)}|^2 p_{\pi(k)}^2 + \frac{\sigma_{UAV}}{\tau_k} \right)$$

$$+ \frac{\sigma_{UAV}}{\tau_k} + \frac{\sigma_{SI}^2}{|g_{\pi(k)}|^2} p_{R,k} p_{\pi(k)}^2 + \frac{\sigma_{UE}}{|g_{\pi(k)}|^2} \frac{p_{R,k}}{\tau_k} \bigg]. \quad (14)$$

In FD-based TWR, the amount of information exchanged by the UE pairs is characterized by

$$R_k(\boldsymbol{\tau}, \mathbf{p}) = \frac{1}{\tau_k} \left[\ln(1 + \gamma_k(\boldsymbol{\tau}, \mathbf{p})) + \ln(1 + \gamma_{\pi(k)}(\boldsymbol{\tau}, \mathbf{p})) \right],$$
$$k = 1, \ldots, K. \quad (15)$$

The problem of maximizing the sum of the information exchanged subject to the constraints of transmit power budget, total bandwidth as well as the QoS for each UE in terms of its throughput is then formulated as[1]

$$\max_{\boldsymbol{\tau}, \mathbf{p}} \sum_{k=1}^{K} R_k(\boldsymbol{\tau}, \mathbf{p}) \quad \text{s.t.} \quad (3), (4), (6), (8), \quad (16a)$$

$$\sum_{k=1}^{K} \frac{1}{\tau_k} \leq 1, \quad (16b)$$

$$\ln(1 + \gamma_\ell(\boldsymbol{\tau}, \mathbf{p})) \geq \bar{r}_\ell \tau_k, \quad (16c)$$
$$\ell \in \{k, \pi(k)\}, \; k = 1, \ldots, K.$$

where (16b) constrains the sum-bandwidth and (16c) sets the QoS for each UE in terms of its throughput thresholds.

By using the slack variable $\boldsymbol{\lambda} \triangleq (\lambda_1, \ldots, \lambda_K)^T \in \mathbb{R}_+^K$, we can express (16) by

$$\max_{\boldsymbol{\tau}, \mathbf{p}, \boldsymbol{\lambda}} \sum_{k=1}^{K} \lambda_k \quad \text{s.t.} \quad (3), (4), (6), (8), (16b), (16c), \quad (17a)$$

$$\ln[1 + \gamma_k(\boldsymbol{\tau}, \mathbf{p})] + \ln[1 + \gamma_{\pi(k)}(\boldsymbol{\tau}, \mathbf{p})] \geq \lambda_k \tau_k, \quad (17b)$$
$$k = 1, \ldots, K.$$

Note that the functions on the left-hand side (LHS) of (17b) and (16c) are nonconcave, making (17) a computationally challenging nonconvex problem. To handle the constraints (17b) and (16c), we develop their new inner approximations, which are based on a lower-bounding concave function approximation for the functions on the LHS of (17b) and (16c) and on an upper-bounding convex function approximation for the RHS of (17b).

Let $(\tau^{(\kappa)}, p^{(\kappa)}, \lambda^{(\kappa)})$ be the feasible point for (17) that is found from the $(\kappa - 1)$th of iteration.

---

[1] For practical implementation, one needs guarding bandwidths between $1/\tau_k$

1) Successive UE throughput function lower bounding approximation: Applying the inequality (77) of Appendix yields

$$\ln[1 + \gamma_k(\boldsymbol{\tau}, \mathbf{p})] \geq$$
$$a_k^{(\kappa)} + b_k^{(\kappa)} p_{\pi(k)} - c_k^{(\kappa)} \bigg[|h_{\pi(k)}|^2 p_{\pi(k)}^2$$

$$+ \frac{\sigma_{SI}^2}{1 - \sigma_{SI}^2} \left(|h_k|^2 p_k^2 + |h_{\pi(k)}|^2 p_{\pi(k)}^2 + \frac{\sigma_{UAV}}{\tau_k} \right)$$

$$+ \frac{\sigma_{UAV}}{\tau_k} + \frac{|\chi_{k,k}|^2}{|g_k|^2} p_{R,k} p_k^2 + \frac{\sigma_{UE}}{|g_k|^2} \frac{p_{R,k}}{\tau_k} \bigg], \quad (18)$$

where

$$0 > a_k^{(\kappa)} = \ln(1 + (\bar{x}_k^{(\kappa)})^2 / \bar{y}_k^{(\kappa)}) - (\bar{x}_k^{(\kappa)})^2 / \bar{y}_k^{(\kappa)},$$
$$0 < b_k^{(\kappa)} = 2\bar{x}_k^{(\kappa)} |h_{\pi(k)}| / \bar{y}_k^{(\kappa)}, \quad (19)$$
$$0 < c_k^{(\kappa)} = (\bar{x}_k^{(\kappa)})^2 / \bar{y}_k^{(\kappa)} ((\bar{x}_k^{(\kappa)})^2 + \bar{y}_k^{(\kappa)}),$$

for

$$\bar{x}_k^{(\kappa)} \triangleq |h_{\pi(k)}| p_{\pi(k)}^{(\kappa)},$$

$$\bar{y}_k^{(\kappa)} \triangleq \frac{\sigma_{SI}^2}{(1 - \sigma_{SI}^2)} \bigg(|h_k|^2 (p_k^{(\kappa)})^2 + |h_{\pi(k)}|^2 (p_{\pi(k)}^{(\kappa)})^2$$

$$+ \frac{\sigma_{UAV}}{\tau_k^{(\kappa)}} \bigg) + \frac{\sigma_{UAV}}{\tau_k^{(\kappa)}} + \frac{|\chi_{k,k}|^2}{|g_k|^2} p_{R,k}^{(\kappa)} (p_k^{(\kappa)})^2$$

$$+ \frac{\sigma_{UE}}{|g_k|^2} \frac{p_{R,k}^{(\kappa)}}{\tau_k^{(\kappa)}}.$$

Furthermore, by using the inequality[2]

$$p_{R,k} \leq \frac{(p_{R,k}^{(\kappa)})^2}{2 p_{R,k}^{(\kappa)} - p_{R,k}}, k = 1, \ldots, K, \quad (20)$$

under the trust region

$$2 p_{R,k}^{(\kappa)} - p_{R,k} \geq 0, k = 1, \ldots, K, \quad (21)$$

it follows that the right-hand side (RHS) of (18) is lower bounded by the following concave function

$$r_k^{(\kappa)}(\boldsymbol{\tau}, \mathbf{p}) \triangleq a_k^{(\kappa)} + b_k^{(\kappa)} p_{\pi(k)} - c_k^{(\kappa)} \bigg[|h_{\pi(k)}|^2 p_{\pi(k)}^2$$

$$+ \frac{\sigma_{SI}^2}{1 - \sigma_{SI}^2} \left(|h_k|^2 p_k^2 + |h_{\pi(k)}|^2 p_{\pi(k)}^2 + \frac{\sigma_{UAV}}{\tau_k} \right)$$

$$+ \frac{\sigma_{UAV}}{\tau_k} + \frac{|\chi_{k,k}|^2}{|g_k|^2} (p_{R,k}^{(\kappa)})^2 \frac{p_k^2}{2 p_{R,k}^{(\kappa)} - p_{R,k}}$$

$$+ \frac{\sigma_{UE}}{|g_k|^2} \frac{(p_{R,k}^{(\kappa)})^2}{(2 p_{R,k}^{(\kappa)} - p_{R,k}) \tau_k} \bigg]. \quad (22)$$

---

[2] $(p_{R,k}^{(\kappa)} - p_{R,k})^2 \geq 0 \Rightarrow (p_{R,k}^{(\kappa)})^2 \geq p_{R,k} \left(2 p_{R,k}^{(\kappa)} - p_{R,k} \right) \Leftrightarrow (20)$ under the trust region (21)

Analogously,

$$\ln\left[1 + \gamma_{\pi(k)}(\boldsymbol{\tau}, \mathbf{p})\right] \geq$$

$$a_{\pi(k)}^{(\kappa)} + b_{\pi(k)}^{(\kappa)} p_k - c_{\pi(k)}^{(\kappa)}\left[|h_k|^2 p_k^2\right.$$

$$+ \frac{\sigma_{SI}^2}{1 - \sigma_{SI}^2}\left(|h_k|^2 p_k^2 + |h_{\pi(k)}|^2 p_{\pi(k)}^2 + \frac{\sigma_{UAV}}{\tau_k}\right)$$

$$+ \frac{\sigma_{UAV}}{\tau_k} + \frac{|\chi_{\pi(k),\pi(k)}|^2}{|g_{\pi(k)}|^2}(p_{R,k}^{(\kappa)})^2 \frac{p_{\pi(k)}^2}{2p_{R,k}^{(\kappa)} - p_{R,k}}$$

$$\left. + \frac{\sigma_{UE}}{|g_{\pi(k)}|^2}\frac{(p_{R,k}^{(\kappa)})^2}{(2p_{R,k}^{(\kappa)} - p_{R,k})\tau_k}\right] \triangleq$$

$$r_{\pi(k)}^{(\kappa)}(\boldsymbol{\tau}, \mathbf{p}), \qquad (23)$$

under the trust region (21), where we have

$$0 > a_{\pi(k)}^{(\kappa)} = \ln(1 + (\bar{x}_{\pi(k)}^{(\kappa)})^2/\bar{y}_{\pi(k)}^{(\kappa)}) - (\bar{x}_{\pi(k)}^{(\kappa)})^2/\bar{y}_{\pi(k)}^{(\kappa)},$$

$$0 < b_{\pi(k)}^{(\kappa)} = 2\bar{x}_{\pi(k)}^{(\kappa)}|h_k|/\bar{y}_{\pi(k)}^{(\kappa)}, \qquad (24)$$

$$0 < c_{\pi(k)}^{(\kappa)} = (\bar{x}_{\pi(k)}^{(\kappa)})^2/\bar{y}_{\pi(k)}^{(\kappa)}((\bar{x}_{\pi(k)}^{(\kappa)})^2 + \bar{y}_{\pi(k)}^{(\kappa)}),$$

for

$$\bar{x}_{\pi(k)}^{(\kappa)} = |h_k| p_k^{(\kappa)},$$

$$\bar{y}_{\pi(k)}^{(\kappa)} = \frac{\sigma_{SI}^2}{(1 - \sigma_{SI}^2)}\left(|h_k|^2 (p_k^{(\kappa)})^2 + |h_{\pi(k)}|^2 (p_{\pi(k)}^{(\kappa)})^2\right.$$

$$\left. + \frac{\sigma_{UAV}}{\tau_k^{(\kappa)}}\right) + \frac{\sigma_{UAV}}{\tau_k^{(\kappa)}} + \frac{|\chi_{\pi(k),\pi(k)}|^2}{|g_{\pi(k)}|^2} p_{R,k}^{(\kappa)}(p_{\pi(k)}^{(\kappa)})^2$$

$$+ \frac{\sigma_{UE}}{|g_{\pi(k)}|^2}\frac{p_{R,k}^{(\kappa)}}{\tau_k^{(\kappa)}}.$$

Since the functions $r_k^{(\kappa)}$ and $r_{\pi(k)}^{(\kappa)}$ are seen to be concave, the nonconvex constraint (16c) in (17) is thus innerly approximated by the following convex constraint

$$r_\ell^{(\kappa)}(\boldsymbol{\tau}, \mathbf{p}) \geq \bar{r}_\ell \tau_k, \ \ell \in \{k, \pi(k)\}, \ k = 1, \dots, K. \qquad (25)$$

Finally, the remaining nonconvex constraint (17b) in (17) is innerly approximated by the following convex constraint

$$r_k^{(\kappa)}(\boldsymbol{\tau}, \mathbf{p}) + r_{\pi(k)}^{(\kappa)}(\boldsymbol{\tau}, \mathbf{p}) \geq \frac{\lambda_k^{(\kappa)} \tau_k^{(\kappa)}}{4}\left(\frac{\lambda_k}{\lambda_k^{(\kappa)}} + \frac{\tau_k}{\tau_k^{(\kappa)}}\right)^2, \quad (26)$$

which exploits the following upper-bounding convex function approximation for the RHS of (17b)

$$\frac{\lambda_k^{(\kappa)} \tau_k^{(\kappa)}}{4}\left(\frac{\lambda_k}{\lambda_k^{(\kappa)}} + \frac{\tau_k}{\tau_k^{(\kappa)}}\right)^2 \geq \lambda_k \tau_k. \qquad (27)$$

2) Path-following algorithm: The following convex problem is solved at the κth iteration to generate the next feasible point $(\tau^{(\kappa+1)}, p^{(\kappa+1)}, \lambda^{(\kappa+1)})$ for the nonconvex problem (17):

$$\max_{\boldsymbol{\tau}, \mathbf{p}, \boldsymbol{\lambda}} \sum_{k=1}^{K} \lambda_k \quad \text{s.t.} \quad (3), (4), (6), (8), (16b), (21), (25), (26).$$
$$(28)$$

The computational complexity of (28) is

$$\mathcal{O}(n^2 m^{2.5} + m^{3.5}), \qquad (29)$$

with $n = 4K$, which is the number of its decision variables, and $m = 7K + 3$, which is the number of its constraints.

Note that $\sum_{k=1}^{K} \lambda_k^{(\kappa)}$ and $\sum_{k=1}^{K} \lambda_k^{(\kappa+1)}$ constitute a feasible value and the optimal value for (28), so

$$\sum_{k=1}^{K} \lambda_k^{(\kappa+1)} > \sum_{k=1}^{K} \lambda_k^{(\kappa)},$$

i.e., the three-tuple $(\tau^{(\kappa+1)}, p^{(\kappa+1)}, \lambda^{(\kappa+1)})$ constitutes a better feasible point for (17) than $(\tau^{(\kappa)}, p^{(\kappa)}, \lambda^{(\kappa)})$ as long as $(\tau^{(\kappa+1)}, p^{(\kappa+1)}) \neq (\tau^{(\kappa)}, p^{(\kappa)})$. As such Algorithm 1, which generates the sequence $\{(\tau^{(\kappa)}, p^{(\kappa)}, \lambda^{(\kappa)})\}$ converges at least to a locally optimal solution of the nonconvex problem (17) [41].

To find an initial feasible point $[\tau^{(0)}, p^{(0)}, \lambda^{(0)}]$ for (17), upon taking any feasible point $(\tau^{(0)}, p^{(0)})$ for the convex constraints (16a) and (16b), we iterate the following convex problem

$$\max_{\boldsymbol{\tau}, \mathbf{p}, \boldsymbol{\lambda}} \min_{k=1,\dots,K} \min_{\ell \in \{k, \pi(k)\}} [r_\ell^{(\kappa)}(\boldsymbol{\tau}, \mathbf{p}) - \bar{r}_\ell \tau_k]$$
$$\text{s.t.} \quad (16a), (16b), (21) \quad (30)$$

until finding the nonnegative optimal value.

Algorithm 1 Path-following algorithm for FD-based TWR

1: **Initialization:** Set $\kappa = 0$. Iterate the convex problem (30) to obtain an initial feasible point $(\tau^{(0)}, p^{(0)}, \lambda^{(0)})$,
2: **Repeat until convergence:** Solve the convex optimization problem (28) to generate the next feasible point $(\tau^{(\kappa+1)}, p^{(\kappa+1)}, \lambda^{(\kappa+1)})$ for (17). Set $\kappa := \kappa + 1$.
3: **Output** $(\tau^{(\kappa)}, p^{(\kappa)})$ as the optimal solution of (17).

III. CONVENTIONAL HALF-DUPLEX TWR

It is quite clear from (13) and (14) that the efficiency of the FD-based TWR is critically dependent on the residual SI attenuation level σ_{SI}, which cannot be suppressed to a level so that the SI in their denominator becomes comparable to the background noise. Furthermore, there are at least two ways of implementing TWR within a single time slot as presented below.

A. Half-time-division (HT) Based TWR

Under this approach, during the first half of the time slot, the UE transmitters send their signals to the UAV and then the UAV relays its received signals to the UE receivers during the other half of the time slot, as depicted in Fig. 2.[3] Hence there is no SI in (13) and (14). The resultant information exchange throughput of UE pairs is given by

$$\frac{1}{2\tau_k}\left[\ln(1 + \tilde{\gamma}_k(\boldsymbol{\tau}, \mathbf{p})) + \ln(1 + \tilde{\gamma}_{\pi(k)}(\boldsymbol{\tau}, \mathbf{p}))\right],$$
$$k = 1, \dots, K, \quad (31)$$

---

[3]If all nodes use the same antennas for signal transmission and reception, a guard time occupying a certain fraction of the TS is required for switching from the transmission mode to the reception mode and vice-versa

instead of (15), where we have

$$\tilde{\gamma}_k(\boldsymbol{\tau}, \mathbf{p}) = |h_{\pi(k)}|^2 p_{\pi(k)}^2 \Big/ \left[\frac{\sigma_{UAV}}{\tau_k} + \frac{\sigma_{UE}}{|g_k|^2} \frac{p_{R,k}}{\tau_k} \right], \quad (32)$$

and

$$\tilde{\gamma}_{\pi(k)}(\boldsymbol{\tau}, \mathbf{p}) = |h_k|^2 p_k^2 \Big/ \left[\frac{\sigma_{UAV}}{\tau_k} + \frac{\sigma_{UE}}{|g_{\pi(k)}|^2} \frac{p_{R,k}}{\tau_k} \right], \quad (33)$$

which represent the SINRs at UE k and UE $\pi(k)$ instead of (13) and (14). The sum information exchange throughput optimization problem corresponding to (17) is formulated as

$$\max_{\boldsymbol{\tau}, \mathbf{p}, \boldsymbol{\lambda}} \quad \sum_{k=1}^{K} \lambda_k \quad \text{s.t.} \quad (3), (4), (16b), (34a)$$

$$\frac{1}{p_{R,k}} \left(|h_k|^2 p_k^2 + |h_{\pi(k)}|^2 p_{\pi(k)}^2 + \frac{\sigma_{UAV}}{\tau_k} \right) \le 2 P^{A,\max}, (34b)$$
$$k = 1, \dots, K,$$

$$\sum_{k=1}^{K} \frac{1}{p_{R,k}} \left(|h_k|^2 p_k^2 + |h_{\pi(k)}|^2 p_{\pi(k)}^2 + \frac{\sigma_{UAV}}{\tau_k} \right)$$
$$\le 4 P_{\text{sum}}^{A,\max}, (34c)$$
$$\ln(1 + \tilde{\gamma}_\ell(\boldsymbol{\tau}, \mathbf{p})) \ge 2\bar{r}_\ell \tau_k, (34d)$$
$$\ell \in \{k, \pi(k)\}, \ k = 1, \dots, K,$$
$$\ln(1 + \tilde{\gamma}_k(\boldsymbol{\tau}, \mathbf{p})) + \ln(1 + \tilde{\gamma}_{\pi(k)}(\boldsymbol{\tau}, \mathbf{p})) \ge 2\lambda_k \tau_k, (34e)$$
$$k = 1, \dots, K,$$

where (34b) and (34c) represent the transmit power at the UAV over the bandwidth $1/\tau_k$ and the sum transmit power of the UAV instead of (6) and (8).
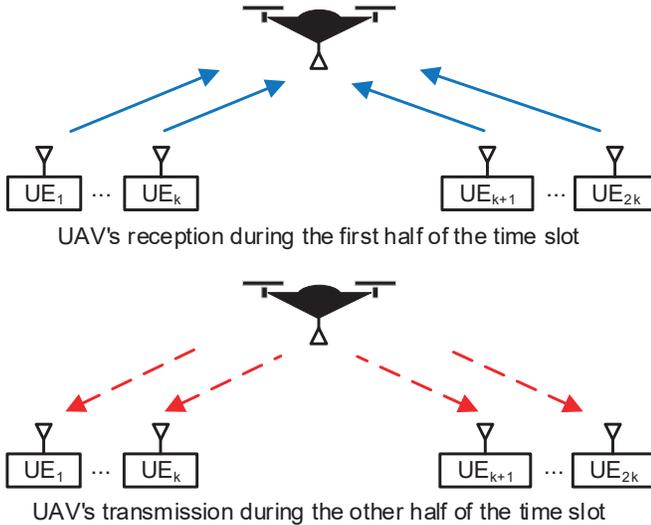
Fig. 2: HT-based TWR

The problem (34) is nonconvex, since the pair of throughput constraints (34d) and (34e) are nonconvex. Let $(\tau^{(\kappa)}, p^{(\kappa)}, \lambda^{(\kappa)})$ represent the feasible point for (34) that is found at the $(\kappa - 1)$th iteration. Similar to (25) and (26), the nonconvex constraints (34d) and (34e) are innerly approximated by the following convex constraints

$$\tilde{r}_\ell^{(\kappa)}(\boldsymbol{\tau}, \mathbf{p}) \ge 2\bar{r}_\ell \tau_k, \ \ell \in \{k, \pi(k)\}, \ k = 1, \dots, K, \quad (35)$$

and

$$\tilde{r}_k^{(\kappa)}(\boldsymbol{\tau}, \mathbf{p}) + \tilde{r}_{\pi(k)}^{(\kappa)}(\boldsymbol{\tau}, \mathbf{p}) \ge \frac{\lambda_k^{(\kappa)} \tau_k^{(\kappa)}}{2} \left(\frac{\lambda_k}{\lambda_k^{(\kappa)}} + \frac{\tau_k}{\tau_k^{(\kappa)}} \right)^2, \quad (36)$$

where we have

$$\tilde{r}_k^{(\kappa)}(\boldsymbol{\tau}, \mathbf{p}, \alpha_k) = a_k^{(\kappa)} + b_k^{(\kappa)} p_{\pi(k)} - c_k^{(\kappa)} \left[|h_{\pi(k)}|^2 p_{\pi(k)}^2 \right.$$
$$\left. + \frac{\sigma_{UAV}}{\tau_k} + \frac{\sigma_{UE}}{|g_k|^2} \frac{(p_{R,k}^{(\kappa)})^2}{(2p_{R,k}^{(\kappa)} - p_{R,k})\tau_k} \right]$$

and

$$\tilde{r}_{\pi(k)}^{(\kappa)}(\boldsymbol{\tau}, \mathbf{p}, \alpha_k) = a_{\pi(k)}^{(\kappa)} + b_{\pi(k)}^{(\kappa)} p_k - c_{\pi(k)}^{(\kappa)} \left[|h_k|^2 p_k^2 \right.$$
$$\left. + \frac{\sigma_{UAV}}{\tau_k} + \frac{\sigma_{UE}}{|g_{\pi(k)}|^2} \frac{(p_{R,k}^{(\kappa)})^2}{(2p_{R,k}^{(\kappa)} - p_{R,k})\tau_k} \right]$$

with $a_k^{(\kappa)}, b_k^{(\kappa)}, c_k^{(\kappa)}$ and $a_{\pi(k)}^{(\kappa)}, b_{\pi(k)}^{(\kappa)}, c_{\pi(k)}^{(\kappa)}$ defined by (19) and (24) for

$$\bar{x}_k^{(\kappa)} \triangleq |h_{\pi(k)}| p_{\pi(k)}^{(\kappa)},$$
$$\bar{y}_k^{(\kappa)} \triangleq \sigma_{UAV}/\tau_k^{(\kappa)} + \sigma_{UE} p_{R,k}^{(\kappa)}/|g_k|^2 \tau_k^{(\kappa)},$$

and

$$\bar{x}_{\pi(k)}^{(\kappa)} \triangleq |h_k| p_k^{(\kappa)},$$
$$\bar{y}_{\pi(k)}^{(\kappa)} \triangleq \sigma_{UAV}/\tau_k^{(\kappa)} + \sigma_{UE} p_{R,k}^{(\kappa)}/|g_{\pi(k)}|^2 \tau_k^{(\kappa)}.$$

At the κ-th iteration we solve the following convex problem to generate the next feasible point $(\tau^{(\kappa+1)}, p^{(\kappa+1)}, \lambda^{(\kappa+1)})$ for the nonconvex problem (34):

$$\max_{\boldsymbol{\tau}, \mathbf{p}, \boldsymbol{\lambda}} \quad \sum_{k=1}^{K} \lambda_k$$
$$\text{s.t.} \ (3), (4), (16b), (21), (34b), (34c), (35), (36). \quad (37)$$

Its computational complexity is (29) with $n = 4K$ and $m = 7K + 3$. Like Algorithm 1, Algorithm 2, which generated the sequence $\{(\tau^{(\kappa)}, p^{(\kappa)}, \lambda^{(\kappa)})\}$, converges at least to a locally optimal solution of the nonconvex problem.

Similarly to (30), upon taking any feasible point $(\tau^{(0)}, p^{(0)})$ for the convex constraints (3), (4), (16b), (34b), and (34c), we iterate the following convex problem

$$\max_{\boldsymbol{\tau}, \mathbf{p}, \boldsymbol{\lambda}} \min_{k=1, \dots, K} \min_{\ell \in \{k, \pi(k)\}} [\tilde{r}_\ell^{(\kappa)}(\boldsymbol{\tau}, \mathbf{p}) - 2\bar{r}_\ell \tau_k]$$
$$\text{s.t.} \quad (3), (4), (16b), (21), (34b), (34c), \quad (38)$$

until obtaining the nonnegative optimal value to locate an initial feasible point $(\tau^{(0)}, p^{(0)}, \lambda^{(0)})$ for (34).

B. Bandwidth partitioning (BP) Based TWR

Under this approach UE k and UE $\pi(k)$ send their signal to the UAV over the bandwidth $1/\tau_k$ and $1/\tau_{\pi(k)}$, respectively.[4] The UAV then relays its received signal to UE $\pi(k)$ and UE

---

[4]Guard bands are necessary for its practical implementation between the adjacent bands of $1/\tau_k$, $k = 1, \dots, 2K$.

Algorithm 2 Path-Following Algorithm for half-time division based HD

1: **Initialization:** Set $\kappa = 0$. Iterate the convex problem (38) for an initial feasible point $(\tau^{(\kappa)}, p^{(\kappa)}, \lambda^{(\kappa)})$ for (34).
2: **Repeat until convergence:** Solve the convex problem (37) to generate the next feasible point $(\tau^{(\kappa+1)}, p^{(\kappa+1)}, \lambda^{(\kappa+1)})$ for (34). Set $\kappa := \kappa + 1$.
3: **Output** $(\tau^{(\kappa)}, p^{(\kappa)})$ as the optimal solution of (34).

k over the same bandwidth fractions with powers $p_{R,\pi(k)}$ and $p_{R,k}$, as depicted in Fig. 3. Then instead of (16b), the bandwidth constraint is

$$\sum_{k=1}^{K} \left(1/\tau_k + 1/\tau_{\pi(k)}\right) \leq 1. \tag{39}$$
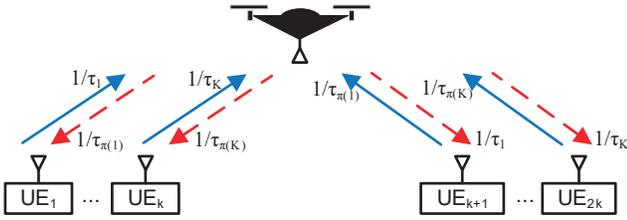
Fig. 3: BP-based TWR

Furthermore, instead of (31), the information exchange throughput of UE pairs is given by

$$\frac{1}{\tau_{\pi(k)}} \ln[1 + \bar{\gamma}_k(\boldsymbol{\tau}, \mathbf{p})] + \frac{1}{\tau_k} \ln[1 + \bar{\gamma}_{\pi(k)}(\boldsymbol{\tau}, \mathbf{p})], \tag{40}$$
$$k = 1, \ldots, K,$$

with

$$\bar{\gamma}_k(\boldsymbol{\tau}, \mathbf{p}) = |h_{\pi(k)}|^2 p_{\pi(k)}^2 \Big/ \left[\frac{\sigma_{UAV}}{\tau_{\pi(k)}} + \frac{\sigma_{UE}}{|g_k|^2} \frac{p_{R,k}}{\tau_{\pi(k)}} \right], \tag{41}$$

and

$$\bar{\gamma}_{\pi(k)}(\boldsymbol{\tau}, \mathbf{p}) = |h_k|^2 p_k^2 \Big/ \left[\frac{\sigma_{UAV}}{\tau_k} + \frac{\sigma_{UE}}{|g_{\pi(k)}|^2} \frac{p_{R,\pi(k)}}{\tau_k} \right]. \tag{42}$$

For $\boldsymbol{\tau} \triangleq \{\tau_k, k = 1, \ldots, \tau_{2K}\}$, $\mathbf{p} = \{(p_k, p_{\pi(k)}, p_{R,k}, p_{R,\pi(k)}), k = 1, \ldots, K\}$, and $\boldsymbol{\lambda} \triangleq \{\lambda_k, k = 1, \ldots, 2K\}$, the problem of sum information exchange throughput optimization corresponding to (34) is

formulated as

$$\max_{\boldsymbol{\tau}, \mathbf{p}, \boldsymbol{\lambda}} \quad \sum_{k=1}^{K} (\lambda_k + \lambda_{\pi(k)}) \quad \text{s.t.} \quad (3), (4), (39), \tag{43a}$$

$$\frac{1}{p_{R,k}} \left(|h_{\pi(k)}|^2 p_{\pi(k)}^2 + \frac{\sigma_{UAV}}{\tau_{\pi(k)}} \right) \leq P^{A,\max}, \tag{43b}$$
$$k = 1, \ldots, K,$$

$$\frac{1}{p_{R,\pi(k)}} \left(|h_k|^2 p_k^2 + \frac{\sigma_{UAV}}{\tau_k} \right) \leq P^{A,\max}, \tag{43c}$$
$$k = 1, \ldots, K,$$

$$\sum_{k=1}^{K} \left(\frac{1}{p_{R,k}} \left(|h_{\pi(k)}|^2 p_{\pi(k)}^2 + \frac{\sigma_{UAV}}{\tau_{\pi(k)}} \right) \right.$$
$$\left. + \frac{1}{p_{R,\pi(k)}} \left(|h_k|^2 p_k^2 + \frac{\sigma_{UAV}}{\tau_k} \right) \right) \leq P^{A,\max}_{\text{sum}}, \tag{43d}$$

$$\ln(1 + \bar{\gamma}_k(\boldsymbol{\tau}, \mathbf{p})) \geq \bar{r}_k \tau_{\pi(k)},$$
$$\ln(1 + \bar{\gamma}_{\pi(k)}(\boldsymbol{\tau}, \mathbf{p})) \geq \bar{r}_{\pi(k)} \tau_k, \ k = 1, \ldots, K, \tag{43e}$$

$$\ln(1 + \bar{\gamma}_k(\boldsymbol{\tau}, \mathbf{p})) \geq \lambda_k \tau_{\pi(k)},$$
$$\ln(1 + \bar{\gamma}_{\pi(k)}(\boldsymbol{\tau}, \mathbf{p})) \geq \lambda_{\pi(k)} \tau_k, \ k = 1, \ldots, K, \tag{43f}$$

where (43b)-(43d) represent the transmit power at the UAV over the bandwidths $1/\tau_{\pi(k)}$ and $1/\tau_k$ and the sum transmit power of UAV instead of (6) and (8). Similarly to (34), (43) is also a nonconvex problem, since the throughput constraints (43e) and (43f) are nonconvex.

Let $(\tau^{(\kappa)}, p^{(\kappa)}, \lambda^{(\kappa)})$ be the feasible point for (43) that is found at the $(\kappa - 1)$th iteration. Similar to (25) and (26), the nonconvex constraints (43e) and (43f) are innerly approximated by the following convex constraints

$$\bar{r}_k^{(\kappa)}(\boldsymbol{\tau}, \mathbf{p}) \geq \bar{r}_k \tau_{\pi(k)}, \ \bar{r}_{\pi(k)}^{(\kappa)}(\boldsymbol{\tau}, \mathbf{p}) \geq \bar{r}_{\pi(k)} \tau_k, \ k = 1, \ldots, K, \tag{44}$$

where we have

$$\bar{r}_k^{(\kappa)}(\boldsymbol{\tau}, \mathbf{p}) \geq \frac{\lambda_k^{(\kappa)} \tau_{\pi(k)}^{(\kappa)}}{4} \left(\frac{\lambda_k}{\lambda_k^{(\kappa)}} + \frac{\tau_{\pi(k)}}{\tau_{\pi(k)}^{(\kappa)}} \right)^2, \ k = 1, \ldots, K, \tag{45a}$$

$$\bar{r}_{\pi(k)}^{(\kappa)}(\boldsymbol{\tau}, \mathbf{p}) \geq \frac{\lambda_{\pi(k)}^{(\kappa)} \tau_k^{(\kappa)}}{4} \left(\frac{\lambda_{\pi(k)}}{\lambda_{\pi(k)}^{(\kappa)}} + \frac{\tau_k}{\tau_k^{(\kappa)}} \right)^2, \ k = 1, \ldots, K, \tag{45b}$$

under the trust region

$$2p_{R,k}^{(\kappa)} - p_{R,k} > 0, k = 1, \ldots, 2K, \tag{46}$$

where we have

$$\bar{r}_k^{(\kappa)}(\boldsymbol{\tau}, \mathbf{p}) = a_k^{(\kappa)} + b_k^{(\kappa)} p_{\pi(k)} - c_k^{(\kappa)} \left[|h_{\pi(k)}|^2 p_{\pi(k)}^2 + \frac{\sigma_{UAV}}{\tau_{\pi(k)}} \right.$$
$$\left. + \frac{\sigma_{UE}}{|g_k|^2} \frac{(p_{R,k}^{(\kappa)})^2}{(2p_{R,k}^{(\kappa)} - p_{R,k})\tau_{\pi(k)}} \right]$$

and

$$\bar{r}_{\pi(k)}^{(\kappa)}(\boldsymbol{\tau}, \mathbf{p}) = a_{\pi(k)}^{(\kappa)} + b_{\pi(k)}^{(\kappa)} p_k - c_{\pi(k)}^{(\kappa)} \left[|h_k|^2 p_k^2 + \frac{\sigma_{UAV}}{\tau_k} \right.$$
$$\left. + \frac{\sigma_{UE}}{|g_{\pi(k)}|^2} \frac{(p_{R,\pi(k)}^{(\kappa)})^2}{(2p_{R,\pi(k)}^{(\kappa)} - p_{R,\pi(k)})\tau_k} \right]$$

with $a_k^{(\kappa)}$, $b_k^{(\kappa)}$, $c_k^{(\kappa)}$ and $a_{\pi(k)}^{(\kappa)}$, $b_{\pi(k)}^{(\kappa)}$, $c_{\pi(k)}^{(\kappa)}$ defined by (19) and (24) for

$$\bar{x}_k^{(\kappa)} \triangleq |h_{\pi(k)}|p_{\pi(k)}^{(\kappa)},$$
$$\bar{y}_k^{(\kappa)} \triangleq \sigma_{UAV}/\tau_{\pi(k)}^{(\kappa)} + \sigma_{UE}p_{R,k}^{(\kappa)}/|g_k|^2\tau_{\pi(k)}^{(\kappa)},$$

and

$$\bar{x}_{\pi(k)}^{(\kappa)} \triangleq |h_k|p_k^{(\kappa)},$$
$$\bar{y}_{\pi(k)}^{(\kappa)} \triangleq \sigma_{UAV}/\tau_k^{(\kappa)} + \sigma_{UE}p_{R,\pi(k)}^{(\kappa)}/|g_{\pi(k)}|^2\tau_k^{(\kappa)}.$$

At the κ-th iteration we solve the following convex problem to generate the next feasible point $(\tau^{(\kappa+1)}, p^{(\kappa+1)}, \lambda^{(\kappa+1)})$ for the nonconvex problem (43)

$$\max_{\boldsymbol{\tau}, \mathbf{p}, \boldsymbol{\lambda}} \quad \sum_{k=1}^{K}(\lambda_k + \lambda_{\pi(k)})$$
s.t. $(3), (4), (39), (43b), (43c), (43d), (44), (45), (46).$ (47)

The computational complexity of (47) is (29) with $n = 6K$ and $m = 10K + 3$. Like Algorithm 1, Algorithm 3, which generates the sequence $\{(\tau^{(\kappa)}, p^{(\kappa)}, \lambda^{(\kappa)})\}$, converges at least to a locally optimal solution of the nonconvex problem (43).

Similarly to (38), upon taking any feasible point $(\tau^{(0)}, p^{(0)})$ for the convex constraints (3), (4), (39), (43b), (43c), and (43d), we iterate the following convex problem

$$\max_{\boldsymbol{\tau}, \mathbf{p}, \boldsymbol{\lambda}} \min_{k=1,\ldots,K} \min\{\bar{r}_k^{(\kappa)}(\boldsymbol{\tau}, \mathbf{p}) - \bar{r}_k\tau_{\pi(k)}, \bar{r}_{\pi(k)}^{(\kappa)}(\boldsymbol{\tau}, \mathbf{p})$$
$$- \bar{r}_{\pi(k)}\tau_k\} \quad \text{s.t.} \quad (3), (4), (39), (43b), (43c), (43d), \quad (48)$$

until obtaining the nonnegative optimal value to locate an initial feasible point $(\tau^{(0)}, p^{(0)})$ for (43).

Algorithm 3 Path-Following Algorithm for bandwidth division based HD

1: **Initialization:** Set $\kappa = 0$. Iterate the convex problem (48) for an initial feasible point $(\tau^{(\kappa)}, p^{(\kappa)}, \lambda^{(\kappa)})$ for (43).
2: **Repeat until convergence:** Solve the convex optimization problem (47) to generate the next feasible point $(\tau^{(\kappa+1)}, p^{(\kappa+1)}, \lambda^{(\kappa+1)})$ for (43). Set $\kappa := \kappa + 1$.
3: **Output** $(\tau^{(\kappa)}, p^{(\kappa)})$ as the optimal solution of (43).

IV. OPTIMAL TIME-FRACTION-BASED (TF) HD TWR

In this section, we propose a TF-based scheme in which the specific time fraction $0 < \mu < 1$ is used for sending information from all UE transmitters to the UAV, while the remaining time fraction of $(1 - \mu)$ is used for forwarding the signals from the UAV to the UE receivers, as depicted in Fig. 4. The hostile loop self-interference inherent in FD-based TWR is thus absent in this TF-based TWR. Assuming that $1/p_k$ is the power share allocated to UE k for sending its information to the UAV. The physical constraint of $1/p_k$ obeys

$$1/p_k \leq \bar{P}_{\text{UE}}, \ 1 \leq k \leq 2K, \quad (49)$$

where $\bar{P}_{\text{UE}} = 3P^{U,\max}$.
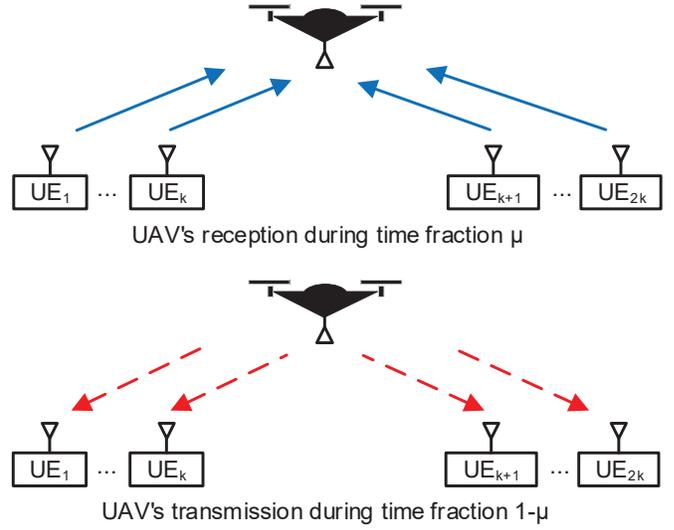
Fig. 4: TF-based TWR

The transmit power constraint of all UEs is

$$\mu \sum_{k=1}^{2K} 1/p_k \leq P_{\text{sum}}^{U,\max}. \quad (50)$$

The signal received by the UAV over the bandwidth $1/\tau_k$ is given by

$$r_k = \sqrt{\mu}\left(\frac{h_k s_k}{\sqrt{p_k}} + \frac{h_{\pi(k)}s_{\pi(k)}}{\sqrt{p_{\pi(k)}}} + n_{R,k}\right). \quad (51)$$

The UAV processes the received signal and applies the transmit power fraction $1/p_{R,k}$ for its transmission

$$\frac{r_k}{\sqrt{p_{R,k}}} = \frac{\sqrt{\mu}}{\sqrt{p_{R,k}}}\left(\frac{h_k s_k}{\sqrt{p_k}} + \frac{h_{\pi(k)}s_{\pi(k)}}{\sqrt{p_{\pi(k)}}} + n_{R,k}\right)$$

which is physically limited by

$$\frac{\mu}{p_{R,k}}\left(\frac{|h_k|^2}{p_k} + \frac{|h_{\pi(k)}|^2}{p_{\pi(k)}} + \frac{\sigma_{UAV}}{\tau_k}\right) \leq \bar{P}_R, \ 1 \leq k \leq K, \quad (52)$$

where we have $\bar{P}_R = 3P^{A,\max}$.

The sum transmit power constraint is formulated as

$$(1-\mu)\mu \sum_{k=1}^{K} \frac{1}{p_{R,k}}\left(\frac{|h_k|^2}{p_k} + \frac{|h_{\pi(k)}|^2}{p_{\pi(k)}} + \frac{\sigma_{UAV}}{\tau_k}\right) \leq P_{\text{sum}}^{R,\max}. \quad (53)$$

Then the signal received by the UEs k and $\pi(k)$ is expressed as

$$y_k = \sqrt{1-\mu}\left[\frac{\sqrt{\mu}}{\sqrt{p_{R,k}}}\left(\frac{h_k s_k}{\sqrt{p_k}} + \frac{h_{\pi(k)}s_{\pi(k)}}{\sqrt{p_{\pi(k)}}} + n_{R,k}\right)\right.$$
$$\left. \times g_k + n_k\right], \quad (54)$$

and

$$y_{\pi(k)} = \sqrt{1-\mu}\left[\frac{\sqrt{\mu}}{\sqrt{p_{R,k}}}\left(\frac{h_k s_k}{\sqrt{p_k}} + \frac{h_{\pi(k)} s_{\pi(k)}}{\sqrt{p_{\pi(k)}}} + n_{R,k}\right)\right.$$
$$\left.\times g_{\pi(k)} + n_{\pi(k)}\right]. \quad (55)$$

The SINR at UE k and $\pi(k)$ after rejecting their own SI is then given by

$$\tilde{\gamma}_k(\boldsymbol{\tau}, \mathbf{p}, \mu) = \frac{\mu|h_{\pi(k)}|^2/p_{R,k}p_{\pi(k)}}{\mu\sigma_{UAV}/p_{R,k}\tau_k + \sigma_{UE}/\tau_k|g_k|^2} \quad (56)$$

and

$$\tilde{\gamma}_{\pi(k)}(\boldsymbol{\tau}, \mathbf{p}, \mu) = \frac{\mu|h_k|^2/p_{R,k}p_k}{\mu\sigma_{UAV}/p_{R,k}\tau_k + \sigma_{UE}/\tau_k|g_{\pi(k)}|^2}. \quad (57)$$

Thus, the infirmation exchange throughput of the UE pairs is defined by

$$R_k(\boldsymbol{\tau}, \mathbf{p}, \mu) = \frac{(1-\mu)}{\tau_k}\left[\ln(1 + \gamma_k(\boldsymbol{\tau}, \mathbf{p}, \mu)) + \ln(1 + \gamma_{\pi(k)}(\boldsymbol{\tau}, \mathbf{p}, \mu))\right] \quad k = 1, \ldots, K. \quad (58)$$

The problem of maximizing the sum information exchange throughput subject to the constraints of our transmit power budget, the total bandwidth and the UEs' throughput is formulated as

$$\max_{\boldsymbol{\tau}, \mathbf{p}, 0<\mu<1} \sum_{k=1}^{K}\frac{(1-\mu)}{\tau_k}\left[\ln(1 + \gamma_k(\boldsymbol{\tau}, \mathbf{p}, \mu))\right.$$
$$\left. + \ln(1 + \gamma_{\pi(k)}(\boldsymbol{\tau}, \mathbf{p}, \mu))\right] \quad (59a)$$
$$\text{s.t.} \quad (16b), (49), (50), (52), (53), \quad (59b)$$
$$\frac{(1-\mu)}{\tau_k}\ln(1 + \gamma_\ell(\boldsymbol{\tau}, \mathbf{p}, \mu)) \geq \bar{r}_\ell, \quad (59c)$$
$$\ell \in \{k, \pi(k)\}, \ k = 1, \ldots, K.$$

Compared to the problem (17), the presence of the new TF variable μ makes the problem (59) much more computationally challenging. Firstly, the UE throughput functions in (59a) are more complex than that in (17b). Secondly, in contrast to the convex constraints (4) and (6), the power constraints (50), (52) and (53) are no longer convex.

For appropriately addressing (59), we first introduce the new variables $\boldsymbol{t} \triangleq (t_1, t_2)$ with $0 < t_1 = 1/\mu$ and $0 < t_2 = 1/(1-\mu)$, satisfying the convex constraint

$$1/t_1 + 1/t_2 \leq 1. \quad (60)$$

Then, (59) is rewritten as

$$\max_{\boldsymbol{\tau}, \mathbf{p}, \boldsymbol{t}} \sum_{k=1}^{K}\frac{1}{\tau_k t_2}\left[\ln(1 + \gamma_k(\boldsymbol{\tau}, \mathbf{p}, \boldsymbol{t}))\right.$$
$$\left. + \ln(1 + \gamma_{\pi(k)}(\boldsymbol{\tau}, \mathbf{p}, \boldsymbol{t}))\right] \quad (61a)$$
$$\text{s.t.} \quad (16b), (49), (60) \quad (61b)$$
$$\sum_{k=1}^{2K}\frac{1}{p_k} \leq P_{\text{sum}}^{U,\max}t_1, \quad (61c)$$
$$\frac{|h_k|^2}{p_{R,k}p_k} + \frac{|h_{\pi(k)}|^2}{p_{R,k}p_{\pi(k)}} + \frac{\sigma_{UAV}}{p_{R,k}\tau_k} \leq \bar{P}_R t_1, \quad (61d)$$
$$1 \leq k \leq K,$$
$$\sum_{k=1}^{K}\left(\frac{|h_k|^2}{t_2 p_{R,k}p_k} + \frac{|h_{\pi(k)}|^2}{t_2 p_{R,k}p_{\pi(k)}} + \frac{\sigma_{UAV}}{t_2 p_{R,k}\tau_k}\right)$$
$$\leq P_{\text{sum}}^{R,\max}t_1, \quad (61e)$$
$$\frac{1}{\tau_k t_2}\ln(1 + \gamma_\ell(\boldsymbol{\tau}, \mathbf{p}, \boldsymbol{t})) \geq \bar{r}_\ell, \quad (61f)$$
$$\ell \in \{k, \pi(k)\}, \ k = 1, \ldots, K,$$

with

$$\gamma_k(\boldsymbol{\tau}, \mathbf{p}, \boldsymbol{t}) = \frac{|h_{\pi(k)}|^2/p_{R,k}p_{\pi(k)}}{\sigma_{UAV}/p_{R,k}\tau_k + \sigma_{UE}t_1/\tau_k|g_k|^2} \quad (62)$$

and

$$\gamma_{\pi(k)}(\boldsymbol{\tau}, \mathbf{p}, \boldsymbol{t}) = \frac{|h_k|^2/p_{R,k}p_k}{\sigma_{UAV}/p_{R,k}\tau_k + \sigma_{UE}t_1/\tau_k|g_{\pi(k)}|^2}. \quad (63)$$

The constraints (61b)-(61e) are convex but the objective function (61a) is nonconcave and the constraint (61f) is nonconvex. Next, we develop a successive lower-bounding approximation for the UE's throughput functions, under which (61f) is innerly approximated by the convex constraint.

Let $(\tau^{(\kappa)}, p^{(\kappa)}, t^{(\kappa)})$ be the feasible point for (61) that is found from the $(\kappa - 1)$th iteration.

A. Successive UE-throughput function lower-bounding approximation

Applying the inequality (76) of Appendix yields

$$\frac{1}{\tau_k t_2}\ln(1 + \gamma_k(\boldsymbol{\tau}, \mathbf{p}, \boldsymbol{t})) \geq$$
$$a_k^{(\kappa)} - b_k^{(\kappa)}\left[\frac{p_{R,k}p_{\pi(k)}}{p_{R,k}^{(\kappa)}p_{\pi(k)}^{(\kappa)}} + c_k^{(\kappa)}\left(\frac{\sigma_{UAV}}{\tau_k p_{R,k}} + \frac{\sigma_{UE}t_1}{|g_k|^2\tau_k}\right)\right]$$
$$- d_k^{(\kappa)}(\frac{t_2}{t_2^{(\kappa)}} + \frac{\tau_k}{\tau_k^{(\kappa)}}), \quad (64)$$

where we have

$$0 < a_k^{(\kappa)} = 3d_k^{(\kappa)} + 2b_k^{(\kappa)},$$
$$0 < b_k^{(\kappa)} = 1/(\bar{x}_k^{(\kappa)}\bar{y}_k^{(\kappa)} + 1)\tau_k^{(\kappa)}t_2^{(\kappa)}$$
$$0 < c_k^{(\kappa)} = 1/\bar{y}_k^{(\kappa)},$$
$$0 < d_k^{(\kappa)} = \ln(1 + 1/\bar{x}_k^{(\kappa)}\bar{y}_k^{(\kappa)})/\tau_k^{(\kappa)}t_2^{(\kappa)},$$

for

$$\bar{x}_k^{(\kappa)} = p_{R,k}^{(\kappa)} p_{\pi(k)}^{(\kappa)}/|h_{\pi(k)}|^2,$$
$$\bar{y}_k^{(\kappa)} = \sigma_{UAV}/\tau_k^{(\kappa)} p_{R,k}^{(\kappa)} + \sigma_{UE} t_1^{(\kappa)}/|g_k|^2 \tau_k^{(\kappa)}.$$

Furthermore, by exploiting the inequalities

$$p_{R,k} p_{\pi(k)} \le \Phi_{\pi(k)}^{(\kappa)}(\mathbf{p}) \triangleq \frac{p_{R,k}^{(\kappa)} p_{\pi(k)}^{(\kappa)}}{4} \left(\frac{p_{R,k}}{p_{R,k}^{(\kappa)}} + \frac{p_{\pi(k)}}{p_{\pi(k)}^{(\kappa)}} \right)^2, \quad (65)$$

and

$$\frac{t_1}{\tau_k} \le \psi_k^{(\kappa)}(\boldsymbol{\tau}, \boldsymbol{t}) \triangleq \frac{t_1^{(\kappa)}}{4\tau_k^{(\kappa)}} \left(\frac{t_1}{t_1^{(\kappa)}} + \frac{\tau_k^{(\kappa)}}{\tau_k} \right)^2, \quad (66)$$

it follows that the RHS of (64) is lower-bounded by the following concave function

$$r_k^{(\kappa)}(\boldsymbol{\tau}, \mathbf{p}, \boldsymbol{t}) \triangleq a_k^{(\kappa)} - b_k^{(\kappa)} \left[\frac{\Phi_{\pi(k)}^{(\kappa)}(\mathbf{p})}{p_{R,k}^{(\kappa)} p_{\pi(k)}^{(\kappa)}} + c_k^{(\kappa)} \left(\frac{\sigma_{UAV}}{\tau_k p_{R,k}} \right. \right.$$
$$\left. \left. + \frac{\sigma_{UE}}{|g_k|^2} \psi_k^{(\kappa)}(\boldsymbol{\tau}, \boldsymbol{t}) \right) \right] - d_k^{(\kappa)} \left(\frac{t_2}{t_2^{(\kappa)}} + \frac{\tau_k}{\tau_k^{(\kappa)}} \right). \quad (67)$$

Analogously, we have

$$\frac{1}{\tau_k t_2} \ln(1 + \gamma_{\pi(k)}(\boldsymbol{\tau}, \mathbf{p}, \boldsymbol{t})) \ge$$

$$a_{\pi(k)}^{(\kappa)} - b_{\pi(k)}^{(\kappa)} \left[\frac{\Phi_k^{(\kappa)}(\mathbf{p})}{p_{R,k}^{(\kappa)} p_k^{(\kappa)}} + c_{\pi(k)}^{(\kappa)} \left(\frac{\sigma_{UAV}}{\tau_k p_{R,k}} \right. \right.$$
$$\left. \left. + \frac{\sigma_{UE}}{|g_{\pi(k)}|^2} \lambda_k^{(\kappa)}(\boldsymbol{\tau}, \boldsymbol{t}) \right) \right] - d_{\pi(k)}^{(\kappa)} \left(\frac{t_2}{t_2^{(\kappa)}} + \frac{\tau_k}{\tau_k^{(\kappa)}} \right) \triangleq$$
$$r_{\pi(k)}^{(\kappa)}(\boldsymbol{\tau}, \mathbf{p}, \boldsymbol{t}), \quad (68)$$

with

$$\Phi_k^{(\kappa)}(\mathbf{p}) \triangleq \frac{p_{R,k}^{(\kappa)} p_k^{(\kappa)}}{4} \left(\frac{p_{R,k}}{p_{R,k}^{(\kappa)}} + \frac{p_k}{p_k^{(\kappa)}} \right)^2, \quad (69)$$

where

$$0 < a_{\pi(k)}^{(\kappa)} = 3d_{\pi(k)}^{(\kappa)} + 2b_{\pi(k)}^{(\kappa)},$$
$$0 < b_{\pi(k)}^{(\kappa)} = 1/(\bar{x}_{\pi(k)}^{(\kappa)} \bar{y}_{\pi(k)}^{(\kappa)} + 1)\tau_k^{(\kappa)} t_2^{(\kappa)},$$
$$0 < c_{\pi(k)}^{(\kappa)} = 1/\bar{y}_{\pi(k)}^{(\kappa)},$$
$$0 < d_{\pi(k)}^{(\kappa)} = \ln(1 + 1/\bar{x}_{\pi(k)}^{(\kappa)} \bar{y}_{\pi(k)}^{(\kappa)})/\tau_k^{(\kappa)} t_2^{(\kappa)},$$

for

$$\bar{x}_{\pi(k)}^{(\kappa)} = p_{R,k}^{(\kappa)} p_k^{(\kappa)}/|h_k|^2,$$
$$\bar{y}_{\pi(k)}^{(\kappa)} = \sigma_{UAV}/\tau_k^{(\kappa)} p_{R,k}^{(\kappa)} + \sigma_{UE} t_1^{(\kappa)}/|g_{\pi(k)}|^2 \tau_k^{(\kappa)}.$$

B. Path-following algorithm

The following convex optimization problem is solved at the κth iteration to generate the next feasible point

$(\tau^{(\kappa+1)}, p^{(\kappa+1)}, t^{(\kappa+1)})$ for the nonconvex problem (59)/(61):

$$\max_{\boldsymbol{\tau}, \mathbf{p}, \boldsymbol{t}} \quad \sum_{k=1}^{K} \left[r_k^{(\kappa)}(\boldsymbol{\tau}, \mathbf{p}, \boldsymbol{t}) + r_{\pi(k)}^{(\kappa)}(\boldsymbol{\tau}, \mathbf{p}, \boldsymbol{t}) \right] \quad (70a)$$
$$\text{s.t.} \quad (61b) - (61e), \quad (70b)$$
$$r_\ell^{(\kappa)}(\boldsymbol{\tau}, \mathbf{p}, \boldsymbol{t}) \ge \bar{r}_\ell, \quad (70c)$$
$$\ell \in \{k, \pi(k)\}, \ k = 1, \ldots, K.$$

The computational complexity of (70) is (29) with $n = 3K+2$ and $m = 4K+4$. Like Algorithm 1, Algorithm 4, which generates the sequence $\{(\tau^{(\kappa)}, p^{(\kappa)}, t^{(\kappa)})\}$, converges at least to a locally optimal solution of the nonconvex problem (59)/(61).

To find an initial feasible point $(\tau^{(0)}, p^{(0)}, t^{(0)})$ for (59) we take any feasible point $(\tau^{(0)}, p^{(0)}, t^{(0)})$ for the convex constraints (61b)-(61e) and iterate the convex problem

$$\max_{\boldsymbol{\tau}, \mathbf{p}, \boldsymbol{t}} \min_{k=1,\ldots,K} \min_{\ell \in \{k, \pi(k)\}} r_\ell^{(\kappa)}(\boldsymbol{\tau}, \mathbf{p}, \boldsymbol{t})/\bar{r}_\ell \quad \text{s.t.} \quad (61b) - (61e),$$
$$(71)$$

until it reaches a value which is more than or equal 1.

Algorithm 4 Path-Following Algorithm for FT
1: **Initialization:** Set $\kappa = 0$. Iterate the convex problem (71) to find an initial feasible point $(\tau^{(0)}, p^{(0)}, t^{(0)})$ for (59).
2: **Repeat until convergence:** Solve the convex optimization problem (70) to generate the next feasible point $(\tau^{(\kappa+1)}, p^{(\kappa+1)})$ for (59). Set $\kappa := \kappa + 1$.
3: **Output** $(\tau^{(\kappa)}, p^{(\kappa)}, t^{(\kappa)})$ as the optimal solution of (59).

V. NUMERICAL RESULTS

This section presents our numerical results characterizing the performance of our algorithms. There are $K = 10$ UEs, which are randomly placed within the cell leaving the cell center at $(100, 50, 0)$ meters, while the remaining $K = 10$ UEs are randomly placed within the cell leaving the cell center at $(-100, 50, 0)$ meters. The radius of the cell is set to 50 meters. The UAV is located at the position of $(0, 50, 200)$ meters. The G2A channel is modelled by

$$h_k = \phi_k \tilde{h}_k, \quad (72)$$

while the A2G channel is modelled by

$$g_k = \varphi_k \tilde{g}_k, \quad (73)$$

where ϕ_k and φ_k denote the large-scale fading coefficients, while $\tilde{h}_k$ and $\tilde{g}_k$ represent the small-scale fading coefficients of the G2A and A2G channel, respectively. The large-scale fading is modelled as log-normal shadowing [42], formulated as

$$PL_k(dB) = PL_0 + 10\alpha \log_{10}(d_k/d_0) + X_\sigma, \quad (74)$$

where $PL_0 = 20 \log_{10}(4\pi d_0 f_c/c)$ is the path loss at the reference distance d_0, the carrier frequency is f_c and the speed of light is $c = 3 \cdot 10^8$ (m/s). Furthermore, α is path loss exponent, which is 2.51 for G2A and 2.32 for A2G [42]–[45], d_k is the distance between UE k and the UAV, and X_σ is a

zero-mean Gaussian distributed random variable with standard deviation σ_X (in dB) representing the shadowing effects.

As there is a dominant line-of-sight path in the propagation channel, the small-scale fading coefficient following the Rician distribution can be modelled as $\tilde{h}_k \sim \mathcal{CN}(\mu, 2\sigma^2)$ with Rician factor $K_R = |\mu|^2/2\sigma^2$. The carrier frequency is $f_c = 2$ GHz, the reference distance is $d_0 = 1$ meter and the Rician factor is $K_R = 10$ [46]. The noise power density is $\sigma_n^2 = -174$ dBm/Hz [11]. Other settings are $P^{U,\max} = 20$ dBm, $P_{\text{sum}}^{U,\max} = KP^{U,\max}$, and $P^{A,\max} = 2P_{\text{sum}}^{R,\max}/K$. The computational tolerance is $\epsilon = 10^{-4}$.

A. Sum information exchange throughput optimization

This subsection analyzes the achievable sum information exchange throughput obtained by four schemes, which are labelled by "FD", "HT", "BP" and "TF" in all figures to refer to FD-based TWR, HT-based TWR, BP-based TWR, and TF-based TWR, respectively.

Figs. 5 and 6 plot the achievable sum information exchange throughput versus SI attenuation level $\sigma_{SI}^2 \in [-150, -110]$ dB for each user throughput threshold of $\bar{r}_\ell \in \{0.1, 0.3, 0.6\}$ bps/Hz. Observe from Fig. 5 that when the value of σ_{SI} is small, which reduces the FD SI to a level similar to noise, FD-based TWR performs significantly better than HT-based TWR and BP-based TWR. However, as the value of σ_{SI} becomes higher and imposes FD SI higher than the noise, the latter outperforms the former, since FD-based TWR fails to eliminate the SI. By contrast, TF-based TWR always achieves better sum information exchange throughput than the other schemes. This is due to the fact that in contrast to TF-based TWR, the time-fractions in HT-based TWR are fixed by definition at $1/2$ without optimization. However, the optimization of the time fraction is not trivial. Furthermore, since all UEs relying on BP-based TWR are allocated separate bandwidths, each member of a pair of UEs has half the bandwidth. This limits their information exchange throughput.

Additionally, we examine the impact of each user throughput threshold $\bar{r}_\ell$ on the sum information exchange throughput. Observe from Fig. 5(a) that the optimal solution of the different schemes satisfies the achievable throughput requirement of each user. However, when $\bar{r}_\ell = 0.3$ bps/Hz, no feasible solution can be found for FD-based TWR associated with $\sigma_{SI}^2 = -110$ dB for satisfying each user's throughput requirement. Under high FD SI conditions it is difficult to make the throughput of each user higher than $\bar{r}_\ell = 0.3$ bps/Hz. Furthermore, when $\bar{r}_\ell = 0.6$ bps/Hz, there are no feasible solutions for BP-based TWR and for HT-based TWR. Indeed, this is also the case for FD-based TWR for $\sigma_{SI}^2 \geq -130$ dB. Furthermore, compared to Fig. 5, the sum information exchange throughput of TF-based TWR and of FD-based TWR in Fig. 6 is reduced a bit, because the feasibility set becomes narrower for higher throughput requirements.

Next, Figs. 7 and 8 plot the achievable sum information exchange throughput versus the UAV transmit power budget of $P_{\text{sum}}^{R,\max}$ for $\bar{r}_\ell \in \{0.1, 0.3, 0.6\}$ bps/Hz. The SI attenuation level is fixed at $\sigma_{SI}^2 = -130$ dB. As expected, the achievable sum information exchange throughput increases with $P_{\text{sum}}^{R,\max}$.

(a) $\bar{r}_\ell = 0.1$

(b) $\bar{r}_\ell = 0.3$
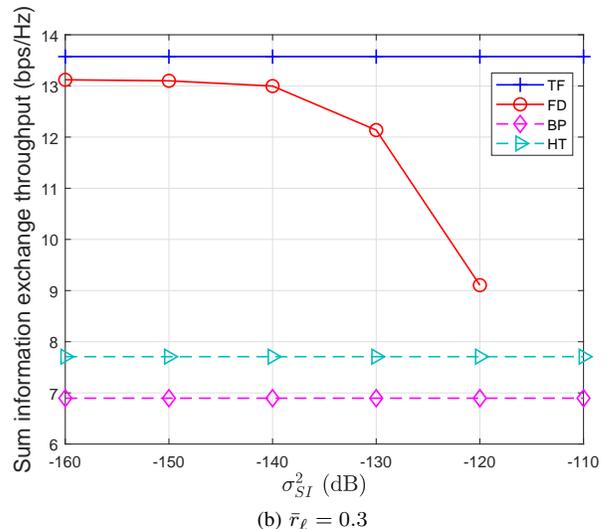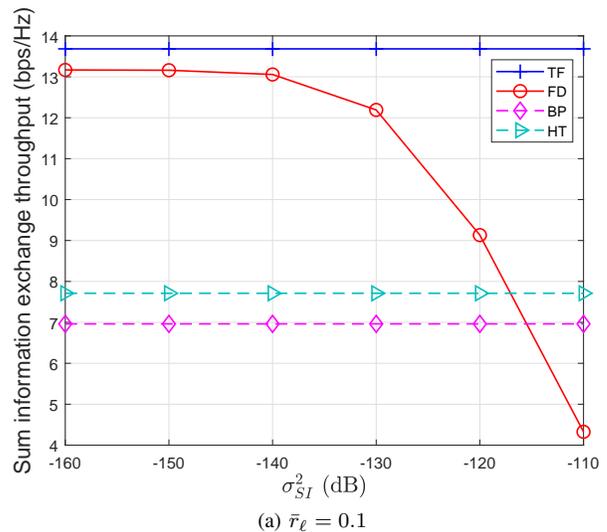
Fig. 5: Sum information exchange throughput versus σ_{SI}^2 as the optimal value of (16) for FD, (34) for HT, (43) for BP, (59) for TF, with $K = 10$ and $\bar{r}_\ell \in \{0.1, 0.3\}$.

The achievable sum information exchange throughput of TF-based TWR is always better than that of the other schemes. Furthermore, observe in Figs. 7 and 8 the gap between TF-based TWR and FD-based TWR is seen wider in $P_{\text{sum}}^{R,\max}$. The increase of $P_{\text{sum}}^{R,\max}$ leads to higher FD SI, thereby hindering the improvement of exchange throughput of FD-based TWR.

Additionally, for $\bar{r}_\ell = 0.1$ bps/Hz, the optimal solution under the different schemes assists each user to satisfy its throughput requirement. However, since we have $\bar{r}_\ell = 0.3$ bps/Hz in Fig. 7(b), no feasible solution can be found for BP-based TWR at $P_{\text{sum}}^{R,\max} = 15$ dBm. Furthermore, when $\bar{r}_\ell$ increases to 0.6 bps/Hz, there are no feasible solutions for BP-based TWR and HT-based TWR. Moreover, no feasible solution can be found for TF-based TWR and FD-based TWR, when $P_{\text{sum}}^{R,\max} = 15$ dBm.

Figs. 9 examines the impact of the number of users K on the sum-rate of information exchange, which increases with K in all schemes. With $P_{\text{sum}}^{R,\max}$ fixed, it is saturated when K
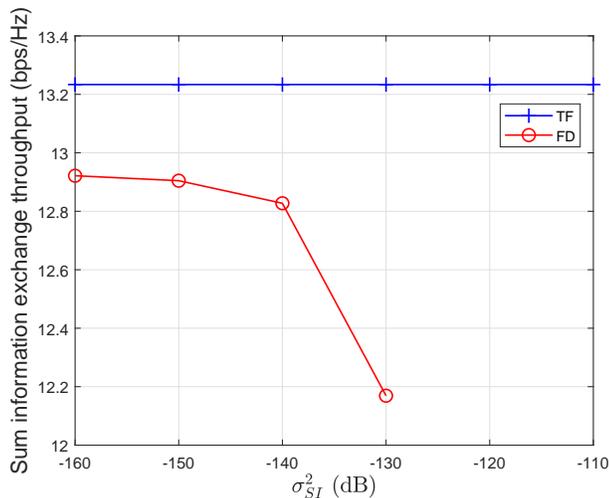
Fig. 6: Sum information exchange throughput versus σ_{SI}^2 as the optimal value of (16) for FD, (34) for HT, (43) for BP, and (59) for TF, with $K = 10$ and $\bar{r}_\ell = 0.6$.

exceeds a certain threshold. Furthermore, Fig. 10, which plots the sum-rate versus the UAV's altitude at $P_{\text{sum}}^{R,\max} = 15$ dBm and $\bar{r}_\ell = 0.1$ bps/Hz, shows that as expected, reducing the power reduces the throughput.

Fig. 11 plots the optimal time fraction μ of TF-based TWR versus the transmit power budget of UAV $P_{\text{sum}}^{R,\max}$ in conjunction with $\bar{r}_\ell = 0.1$ bps/Hz. It can be seen that the time fraction μ, which is used for sending information from all UEs to the UAV, decreases when $P_{\text{sum}}^{R,\max}$ increases. Given a higher power budget, an increased time fraction is allocated to the link spanning from the UAV to the UEs.

Fig. 12 plots the bandwidth allocations $1/\tau_k$ associated with $\bar{r}_\ell = 0.1$ bps/Hz. All UEs are allocated separate bandwidths in BP-based TWR, while UEs k and $\pi(k)$ share the fraction $1/\tau_k$ of bandwidth in the other schemes. The bandwidths allocated to UE pairs $(6, 16)$ and $(9, 19)$ are much higher than that allocated to other UE pairs, because the channel gains g_k in the UE pairs of $(6, 16)$ and $(9, 19)$ are stronger than that of other UE pairs, indicating that the sum information throughput optimization may assign more bandwidth to strong UE pairs. Next, Figs. 13(a) and 13(b) plot the optimal transmit power allocation for the UEs to the UAV link and for the UAV to UEs link, respectively. As seen in Fig. 13, the transmit power allocation for the link spanning from the UEs to the UAV under TF-based TWR is lower than that under the other schemes, but the former needs more power for its transmission from the UAV to UEs. This explains why TF-based TWR significantly outperforms the other schemes in terms of its sum information exchange throughput.

B. Algorithmic convergence

Fig. 14 characterizes the four algorithms convergence. The HT-based TWR algorithm achieves the fastest convergence rate. The BP-based TWR and FD-based TWR algorithms require 23 and 30 iterations, respectively, whereas TF-based TWR needs more iterations.
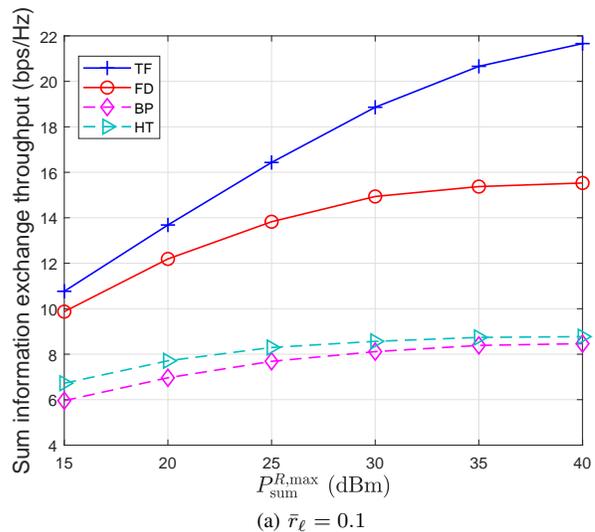
(a) $\bar{r}_\ell = 0.1$
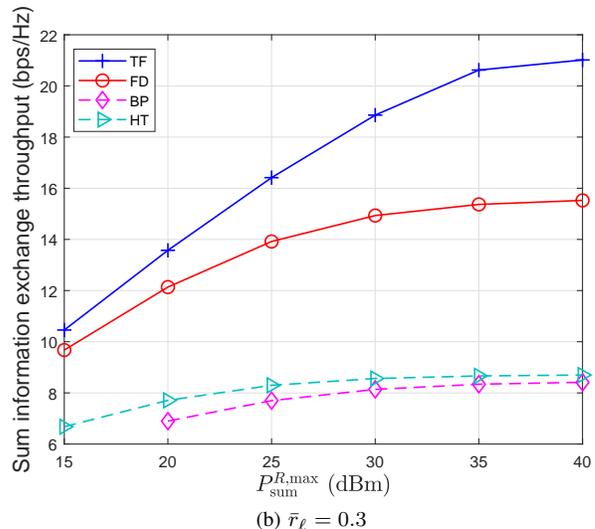
(b) $\bar{r}_\ell = 0.3$

Fig. 7: Sum information exchange throughput versus $P_{\text{sum}}^{R,\max}$ with $K = 10$ as the optimal value of (16) for FD, (34) for HT, (43) for BP, and (59) for TF

VI. CONCLUSIONS

Four UAV-aided TWR solutions have been conceived, where pairs of users can exchange information via the UAV relay. A pair of prospective approaches have been proposed to enable information exchange between pairs of users within one time slot. The first approach is FD-based TWR, which relies on FD transceivers both at the UAV relay and at the users, while the second approach is TF-aided HD TWR, which allows both the UAV relay and users to employ a fraction of the time to transmit and receive. In contrast to the first approach, it is much easier to implement the second one for UAV-enabled TWR. The problems of jointly optimizing both the bandwidth and power allocation for pairs of users to maximize minimum information exchange throughput have been solved by our efficient path-following algorithms with the aid of new inner approximation techniques. Our numerical results show the advantage of TF-based HD TWR over conventional HD
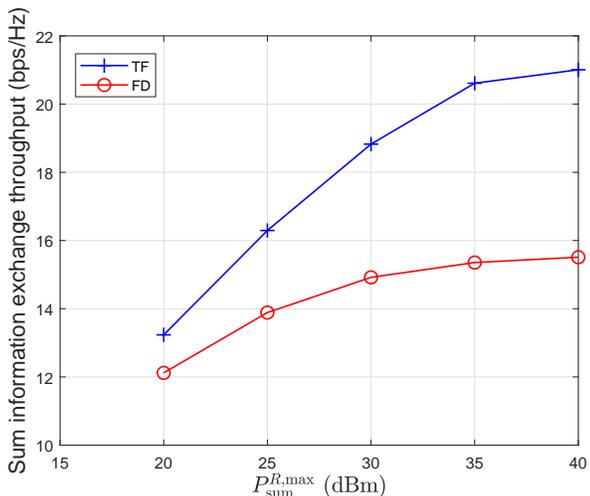
Fig. 8: Sum information exchange throughput versus $P_{\text{sum}}^{R,\max}$ with $K = 10$ and $\bar{r}_\ell = 0.6$ as the optimal value of (16) for FD, (34) for HT, (43) for BP, and (59) for TF

Fig. 10: Sum information exchange throughput versus the UAV altitude with $P_{\text{sum}}^{R,\max} = 15$ dBm and $\bar{r}_\ell = 0.1$ as the optimal value of (16) for FD, (34) for HT, (43) for BP, and (59) for TF

Fig. 9: Sum information exchange throughput versus K with $P_{\text{sum}}^{R,\max} = 15$ dBm and $\bar{r}_\ell = 0.1$ as the optimal value of (16) for FD, (34) for HT, (43) for BP, and (59) for TF
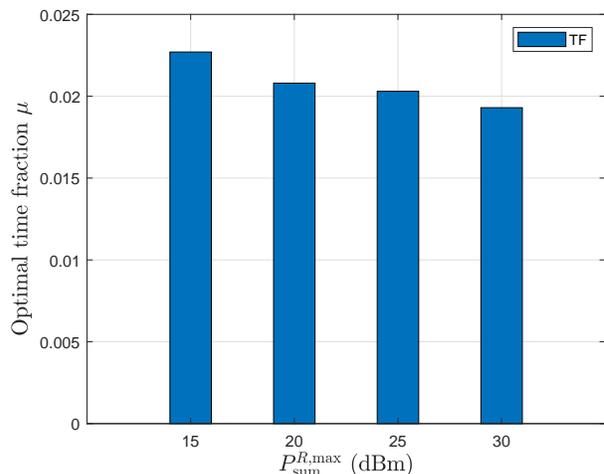
Fig. 11: Optimal time fraction μ versus $P_{\text{sum}}^{R,\max}$ with $K = 10$ and $\bar{r}_\ell = 0.1$.

TWR and FD-based TWR.

APPENDIX: FUNDAMENTAL INEQUALITIES

The following inequalities were proved in [36] and [47]:

$$\frac{\ln(1+1/xy)}{zt} \geq 3\frac{\ln(1+1/\bar{x}\bar{y})}{\bar{z}\bar{t}} + \frac{1}{(\bar{x}\bar{y}+1)\bar{z}\bar{t}}\left(2 - \frac{x}{\bar{x}} - \frac{y}{\bar{y}}\right)$$
$$- \frac{\ln(1+1/\bar{x}\bar{y})}{\bar{z}^2\bar{t}}z - \frac{\ln(1+1/\bar{x}\bar{y})}{\bar{z}\bar{t}^2}t, \quad (75)$$

and

$$\frac{1}{\tau}\ln(1+1/xy) \geq \frac{2}{\bar{\tau}}\ln(1+1/\bar{x}\bar{y}) + \frac{1}{(1+\bar{x}\bar{y})\bar{\tau}}\left(2 - \frac{x}{\bar{x}} - \frac{y}{\bar{y}}\right)$$
$$- \frac{\ln(1+1/\bar{x}\bar{y})}{\bar{\tau}^2}\tau. \quad (76)$$

for all $x > 0$, $y > 0$, $z > 0$, $t > 0$, and $\bar{x} > 0$, $\bar{y} > 0$, $\bar{z} > 0$, $\bar{t} > 0$, while

$$\ln(1+x^2/y) \geq \ln(1+\bar{x}^2/\bar{y}) - \frac{\bar{x}^2}{\bar{y}} + 2\frac{\bar{x}}{\bar{y}}x - \frac{\bar{x}^2}{\bar{y}(\bar{y}+\bar{x}^2)}(x^2+y) \quad (77)$$

for all $x \geq 0$, $y > 0$, and $\bar{x} \geq 0$, $\bar{y} > 0$.

REFERENCES

[1] Y. Zeng, R. Zhang, and T. J. Lim, "Wireless communications with unmanned aerial vehicles: Opportunities and challenges," *IEEE Commun. Mag.*, vol. 54, no. 5, pp. 36–42, 2016.

[2] L. Gupta, R. Jain, and G. Vaszkun, "Survey of important issues in UAV communication networks," *IEEE Commun. Surveys Tuts.*, vol. 18, no. 2, pp. 1123–1152, 2016.

[3] M. Mozaffari, W. Saad, M. Bennis, and M. Debbah, "Mobile unmanned aerial vehicles (UAVs) for energy-efficient internet of things communications," *IEEE Trans. Wirel. Commun.*, vol. 16, no. 11, pp. 7574–7589, Nov. 2017.
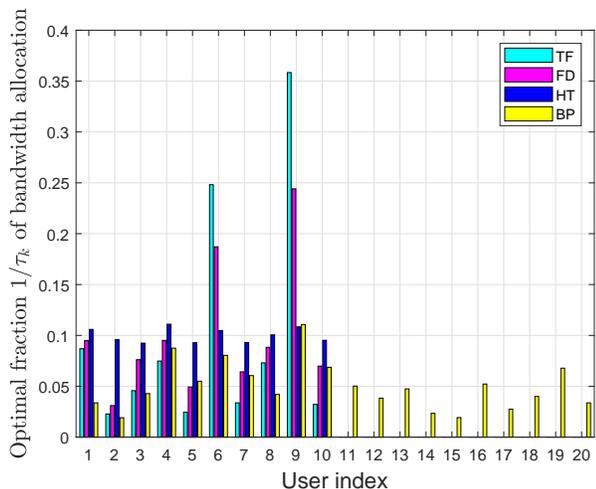
Fig. 12: Optimal fraction $1/\tau_k$ of bandwidth allocation with $K = 10$ and $\bar{r}_\ell = 0.1$.

Fig. 14: Convergence of the proposed Algorithms.
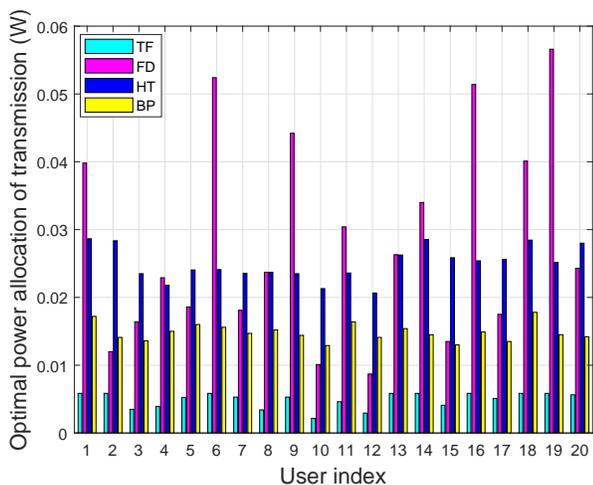
(a) Transmission from UEs to the UAV.
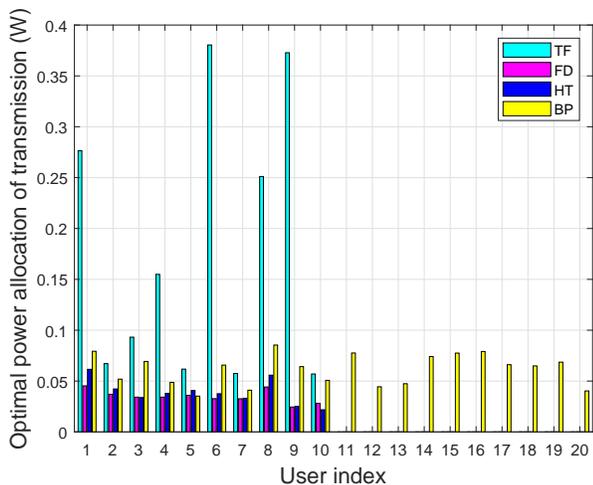
(b) Transmission from the UAV to UEs.

Fig. 13: Optimal power allocation

[4] X. Lin *et al.*, "The sky is not the limit: LTE for unmanned aerial vehicles," *IEEE Commun. Mag.*, vol. 56, no. 4, pp. 204–210, 2018.

[5] N. Zhao, W. Lu, M. Sheng, Y. Chen, J. Tang, F. R. Yu, and K.-K. Wong, "UAV-assisted emergency networks in disasters," *IEEE Wirel. Commun.*, vol. 26, no. 1, pp. 45–51, Feb. 2019.

[6] X. Liu, Y. Liu, Y. Chen, and L. Hanzo, "Trajectory design and power control for multi-UAV assisted wireless networks: A machine learning approach," *IEEE Trans. Veh. Technol.*, vol. 68, no. 8, pp. 7957–7969, Aug 2019.

[7] X. Li, H. Yao, J. Wang, X. Xu, C. Jiang, and L. Hanzo, "A near-optimal UAV-aided radio coverage strategy for dense urban areas," *IEEE Trans. Veh. Technol.*, vol. 68, no. 9, pp. 9098–9109, Sep. 2019.

[8] H. T. Nguyen, H. D. Tuan, T. Q. Duong, H. V. Poor, and W.-J. Hwang, "Joint D2D assignment, bandwidth and power allocation in cognitive UAV-enabled networks," *IEEE Trans. Cogn. Commun. Network. (early access)*.

[9] Z. Sheng, H. D. Tuan, A. A. Nasir, T. Q. Duong, and H. V. Poor, "Secure UAV-enabled communication using Han-Kobayashi signaling," *IEEE Trans. Wirel. Commun.*, vol. 19, no. 5, pp. 2905–2919, 2020.

[10] H. He, S. Zhang, Y. Zeng, and R. Zhang, "Joint altitude and beamwidth optimization for UAV-enabled multiuser communications," *IEEE Commun. Lett.*, vol. 22, no. 2, pp. 344–347, 2018.

[11] R. Fan, J. Cui, S. Jin, K. Yang, and J. An, "Optimal node placement and resource allocation for UAV relaying network," *IEEE Commun. Lett.*, vol. 22, no. 4, pp. 808–811, 2018.

[12] A. A. Nasir, H. D. Tuan, T. Q. Duong, and H. V. Poor, "UAV-enabled communication using NOMA," *IEEE Trans. Commun.*, vol. 67, no. 7, pp. 5126–5138, 2019.

[13] W. Huang, D. M. Kim, W. Ding, and P. Popovski, "Joint optimization of altitude and transmission direction in UAV-based two-way communication," *IEEE Wirel. Commun. Lett.*, vol. 8, no. 4, pp. 984–987, 2019.

[14] B. Duo, Q. Wu, X. Yuan, and R. Zhang, "Energy efficiency maximization for full-duplex UAV secrecy communication," *IEEE Trans. Veh. Technol.*, vol. 69, no. 4, pp. 4590–4595, 2020.

[15] Y. Zeng, R. Zhang, and T. J. Lim, "Throughput maximization for UAV-enabled mobile relaying systems," *IEEE Trans. Commun.*, vol. 64, no. 12, pp. 4983–4996, 2016.

[16] S. Zhang, H. Zhang, Q. He, K. Bian, and L. Song, "Joint trajectory and power optimization for UAV relay networks," *IEEE Commun. Lett.*, vol. 22, no. 1, pp. 161–164, 2018.

[17] X. Jiang, Z. Wu, Z. Yin, and Z. Yang, "Joint power and trajectory design for UAV-relayed wireless systems," *IEEE Wirel. Commun. Lett.*, vol. 8, no. 3, pp. 697–700, 2019.

[18] Y. Chen, N. Zhao, Z. Ding, and M.-S. Alouini, "Multiple UAVs as relays: Multi-hop single link versus multiple dual-hop links," *IEEE Trans. Wirel. Commun.*, vol. 17, no. 9, pp. 6348–7363, Sept. 2018.

[19] Y. Takahashi, Y. Kawamoto, H. Nishiyama, N. Kato, F. Ono, and R. Miura, "A novel radio resource optimization method for relay-based unmanned aerial vehicles," *IEEE Trans. Wirel. Commun.*, no. 11, pp. 7532–7363, Nov. 2018.

[20] B. Rankov and A. Wittneben, "Spectral efficient protocols for half-duplex fading relay channels," *IEEE J. Sel. Areas Commun.*, vol. 25, no. 2, pp. 379–389, 2007.

[21] S. Katti, S. Gollakota, and D. Katabi, "Embracing wireless interference: Analog network coding," in *Proc. ACM SIGCOMM*, vol. 37, no. 4, 2007, pp. 397–408.

[22] P. Popovski and H. Yomo, "Wireless network coding by amplify-and-forward for bi-directional traffic flows," *IEEE Commun. Lett.*, vol. 11, no. 1, pp. 16–18, 2007.

[23] D. Gunduz, A. Yener, A. Goldsmith, and H. V. Poor, "The multiway relay channel," *IEEE Trans. Inf. Theory*, vol. 59, no. 1, pp. 51–63, 2012.

[24] Z. Sheng, H. D. Tuan, T. Q. Duong, and H. V. Poor, "Joint power allocation and beamforming for energy-efficient two-way multi-relay communications," *IEEE Trans. Wirel. Commun.*, vol. 16, no. 10, pp. 6660–6671, Oct. 2017.

[25] L. Li, T. Chang, and S. Cai, "UAV positioning and power control for two-way wireless relaying," *IEEE Trans. Wirel. Commun.*, vol. 19, no. 2, pp. 1008–1024, 2020.

[26] S. Eom, H. Lee, J. Park, and I. Lee, "UAV-aided two-way mobile relaying systems," *IEEE Commun. Lett.*, vol. 24, no. 2, pp. 438–442, 2020.

[27] Y.-S. Choi and H. Shirani-Mehr, "Simultaneous transmission and reception: Algorithm, design and system level performance," *IEEE Trans. Wirel. Commun.*, vol. 12, no. 12, pp. 5992–6010, 2013.

[28] S. Hong, J. Brand, J. I. Choi, M. Jain, J. Mehlman, S. Katti, and P. Levis, "Applications of self-interference cancellation in 5G and beyond," *IEEE Commun. Mag.*, vol. 52, no. 2, pp. 114–121, 2014.

[29] E. Everett, A. Sahai, and A. Sabharwal, "Passive self-interference suppression for full-duplex infrastructure nodes," *IEEE Trans. Wirel. Commun.*, vol. 13, no. 2, pp. 680–694, 2014.

[30] V. Syrjala, M. Valkama, L. Anttila, T. Riihonen, and D. Korpi, "Analysis of oscillator phase-noise effects on self-interference cancellation in full-duplex OFDM radio transceivers," *IEEE Trans. Wirel. Commun.*, vol. 13, no. 6, pp. 2977–2990, 2014.

[31] S. Li and R. D. Murch, "An investigation into baseband techniques for single-channel full-duplex wireless communication systems," *IEEE Trans. Wirel. Commun.*, vol. 13, no. 9, pp. 4794–4806, 2014.

[32] L. Li, C. Dong, L. Wang, and L. Hanzo, "Spectral-efficient bidirectional decode-and-forward relaying for full-duplex communication," *IEEE Trans. Veh. Technol.*, vol. 65, no. 9, pp. 7010–7020, Sep. 2016.

[33] E. Sharma, R. Budhiraja, K. Vasudevan, and L. Hanzo, "Full-duplex massive MIMO multi-pair two-way AF relaying: Energy efficiency optimization," *IEEE Trans. Commun.*, vol. 66, no. 8, pp. 3322–3340, Aug 2018.

[34] H. H. M. Tam, H. D. Tuan, and D. T. Ngo, "Successive convex quadratic programming for quality-of-service management in full-duplex MU-MIMO multicell networks," *IEEE Trans. Commun.*, vol. 64, no. 6, pp. 2340–2353, 2016.

[35] Z. Sheng, H. D. Tuan, H. H. M. Tam, H. H. Nguyen, and Y. Fang, "Energy-efficient precoding in multicell networks with full-duplex base stations," *EURASIP J. Wirel. Commun. Networking*, 2017, DOI 10.1186/s13638-017-0831-5.

[36] Z. Sheng, H. D. Tuan, T. Q. Duong, H. V. Poor, and Y. Fang, "Low-latency multiuser two-way wireless relaying for spectral and energy efficiencies," *IEEE Trans. Signal Process.*, vol. 66, no. 16, pp. 4362–4376, 2018.

[37] A. A. Nasir, H. D. Tuan, and T. Q. Duong, "Fractional time exploitation for serving IoT users with guaranteed QoS by 5G spectrum," *IEEE Commun. Mag.*, vol. 56, no. 10, pp. 128–133, 2018.

[38] L. Wang and L. Hanzo, "Optimum time resource allocation for TDMA-based differential decode-and-forward cooperative systems: a capacity perspective," *IEEE Commun. Lett.*, vol. 14, no. 6, pp. 506–508, Jun. 2010.

[39] L. Wang, L. Li, C. Xu, D. Liang, S. X. Ng, and L. Hanzo, "Multiple-symbol joint signal processing for differentially encoded single- and multi-carrier communications: Principles, designs and applications," *IEEE Commun. Surveys & Tuts.*, vol. 16, no. 2, pp. 689–712, 2nd quarter 2014.

[40] M. Asadpour, B. van den Bergh, D. Giustiniano, K. Hummel, S. Pollin, and B. Plattner, "Micro aerial vehicle networks: An experimental analysis of challenges and opportunities," *IEEE Commun. Mag.*, vol. 52, no. 7, pp. 141–149, 2014.

[41] B. R. Marks and G. P. Wright, "A general inner approximation algorithm for nonconvex mathematical programs," *Operations Research*, vol. 26, no. 4, pp. 681–683, Jul 1978.

[42] N. Ahmed, S. S. Kanhere, and S. Jha, "On the importance of link characterization for aerial wireless sensor networks," *IEEE Commun. Mag.*, vol. 54, no. 5, pp. 52–57, 2016.

[43] *Study on Enhanced LTE Support for Aerial Vehicles.* v15.0.0, document TR 36.777, 3GPP, Dec. 2017.

[44] A. A. Khuwaja, Y. Chen, N. Zhao, and M.-S. A. P. Dobbins, "A survey of channel modeling for UAV communications," *IEEE Commun. Surveys & Tuts.*, vol. 20, no. 4, pp. 2804–2821, 4th Quart. 2018.

[45] W. Khawaja, I. Guvenc, D. W. Matolak, U.-C. Fiebig, and N. Schneckenburger, "A survey of air-to-ground propagation channel modeling for unmanned aerial vehicles," *IEEE Commun. Surveys & Tuts.*, vol. 21, no. 3, pp. 2361–2391, 3rd Quart. 2019.

[46] F. Ono, H. Ochiai, and R. Miura, "A wireless relay network based on unmanned aircraft system with rate optimization," *IEEE Trans. Wirel. Commun.*, vol. 15, no. 11, pp. 7699–7708, Nov. 2016.

[47] Z. Sheng, H. D. Tuan, A. A. Nasir, T. Q. Duong, and H. V. Poor, "Power allocation for energy efficiency and secrecy of wireless interference networks," *IEEE Trans. Wirel. Commun.*, vol. 17, no. 6, pp. 3737–3751, Jun. 2018.

Zhichao Sheng received the Ph.D. degree in electrical engineering from the University of Technology, Sydney, NSW, Australia in 2018. From 2018 to 2019, he was a Research Fellow at School of Electronics, Electrical Engineering and Computer Science, Queen's University Belfast, Belfast, U.K. He is currently a Lecturer with Shanghai University, Shanghai, China. His research interests include optimization methods for wireless communication and signal processing.

Hoang Duong Tuan received the Diploma (Hons.) and Ph.D. degrees in applied mathematics from Odessa State University, Ukraine, in 1987 and 1991, respectively. He spent nine academic years in Japan as an Assistant Professor in the Department of Electronic-Mechanical Engineering, Nagoya University, from 1994 to 1999, and then as an Associate Professor in the Department of Electrical and Computer Engineering, Toyota Technological Institute, Nagoya, from 1999 to 2003. He was a Professor with the School of Electrical Engineering and Telecommunications, University of New South Wales, from 2003 to 2011. He is currently a Professor with the School of Electrical and Data Engineering, University of Technology Sydney. He has been involved in research with the areas of optimization, control, signal processing, wireless communication, and biomedical engineering for more than 20 years.

Trung Q. Duong (S'05, M'12, SM'13) received his Ph.D. degree in Telecommunications Systems from Blekinge Institute of Technology (BTH), Sweden in September 2012. Currently, he is a Research Chair - Royal Academy of Engineering and a Professor with Queen's University Belfast (UK), where he was a Lecturer (Assistant Professor) (2013-2017), a Reader (Associate Professor) (2018-2020), and Full Professor from August 2020. His current research interests include wireless communications, machine learning, realtime optimisation, big data, and IoT applications to disaster management, air-quality monitoring, flood monitoring, smart agriculture, healthcare and smart cities. He is the author or co-author of over 350+ technical papers published in scientific journals (230+ articles) and presented at international conferences (140+ papers).

Dr. Duong currently serves as an Editor for the IEEE TRANSACTIONS ON WIRELESS COMMUNICATIONS, IEEE TRANSACTIONS ON COMMUNICATIONS, and an Executive Editor for IEEE COMMUNICATIONS LETTERS. He was awarded the Best Paper Award at the IEEE Vehicular Technology Conference (VTC-Spring) in 2013, IEEE International Conference on Communications (ICC) 2014, IEEE Global Communications Conference (GLOBECOM) 2016 and 2019, IEEE Digital Signal Processing Conference (DSP) 2017, and International Wireless Communications & Mobile Computing Conference (IWCMC) 2019. He is the recipient of prestigious Royal Academy of Engineering Research Fellowship (2015-2020) and has won a prestigious Newton Prize 2017.

Lajos Hanzo (http://www-mobile.ecs.soton.ac.uk, https://en.wikipedia.org/wiki/Lajos_Hanzo) (FIEEE'04, Fellow of the Royal Academy of Engineering F(REng), of the IET and of EURASIP), received his Master degree and Doctorate in 1976 and 1983, respectively from the Technical University (TU) of Budapest. He was also awarded the Doctor of Sciences (DSc) degree by the University of Southampton (2004) and Honorary Doctorates by the TU of Budapest (2009) and by the University of Edinburgh (2015). He is a Foreign Member of the Hungarian Academy of Sciences and a former Editor-in-Chief of the IEEE Press. He has served several terms as Governor of both IEEE ComSoc and of VTS. He has published 1900+ contributions at IEEE Xplore, 19 Wiley-IEEE Press books and has helped the fast-track career of 123 PhD students. Over 40 of them are Professors at various stages of their careers in academia and many of them are leading scientists in the wireless industry.